5. Results and Discussion

5.1. Pre-formulation Studies

5.1.1. Development of analytical method for the estimation of ciprofloxacin hydrochloride and quercetin by UV-Vis spectroscopy

5.1.1.1. Determination of λ_{max}

The individual UV-Vis spectra of ciprofloxacin hydrochloride (CH) and quercetin (Que) in phosphate buffer (pH 7.4) are shown in Figure 5.1. The spectra of CH and Que exhibited a sharp peak at 271 nm and 370 nm, respectively. In addition, both the drugs showed two nearby distinct sharp peaks which lose its sharpness at low concentration. Therefore, an absorbance maximum (λ_{max}) for CH and Que estimation was selected at 271 nm and 370 nm, respectively. CH and Que are UV-Visible active drugs and display distinct absorption maximum that is well separated from each other. However, they cannot be quantitatively determined by direct UV-Vis spectroscopic technique in mixed solution owing to the masking of λ_{max} of one drug with the other drug absorbance curve. Therefore, simultaneous-equation, an indirect method was developed and validated in phosphate buffer (pH 7.4) for simultaneous estimation of both drugs.

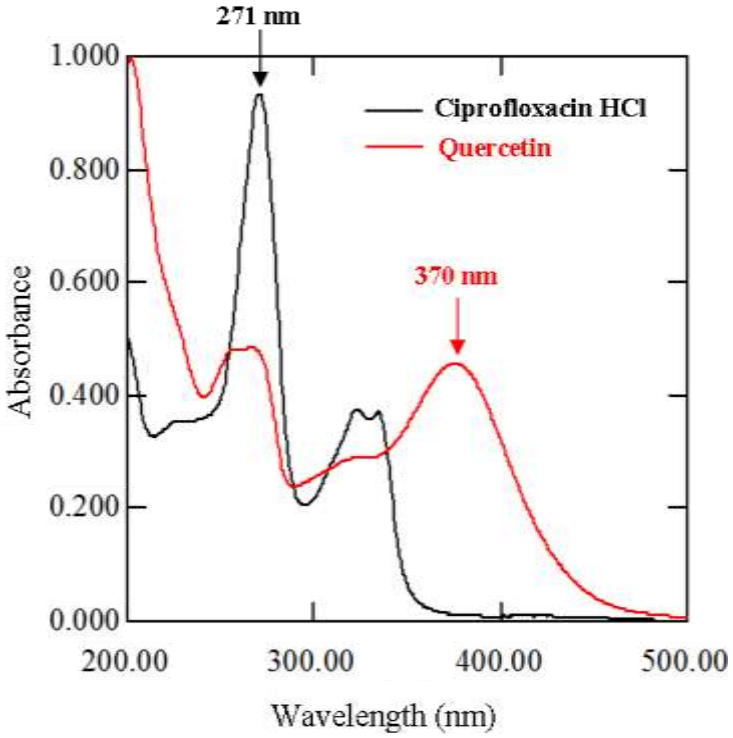

Figure 5.1: Overlay spectra of ciprofloxacin hydrochloride and quercetin

5.1.1.2. Preparation of calibration curve in phosphate buffer (pH7.4) and determination of related parameters

Standard calibration curve of CH and Que was obtained in phosphate buffer (pH7.4) after plotting concentration versus absorbance at λ_{max} 271nm and 370nm, respectively. The overlay spectra of different concentrations and respective standard curve for CH and Que are shown in Figures 5.2 and 5.3, respectively. It was observed that Beer's & Lambert's law was obeyed in the selected concentration and a straight line with high regression coefficient (>0.999) was obtained. The high regression value indicated the high linearity between chosen concentration and absorbance. The concentration range, regression equation, regression coefficient and obtained molar absorptivity are given in Table 5.1.

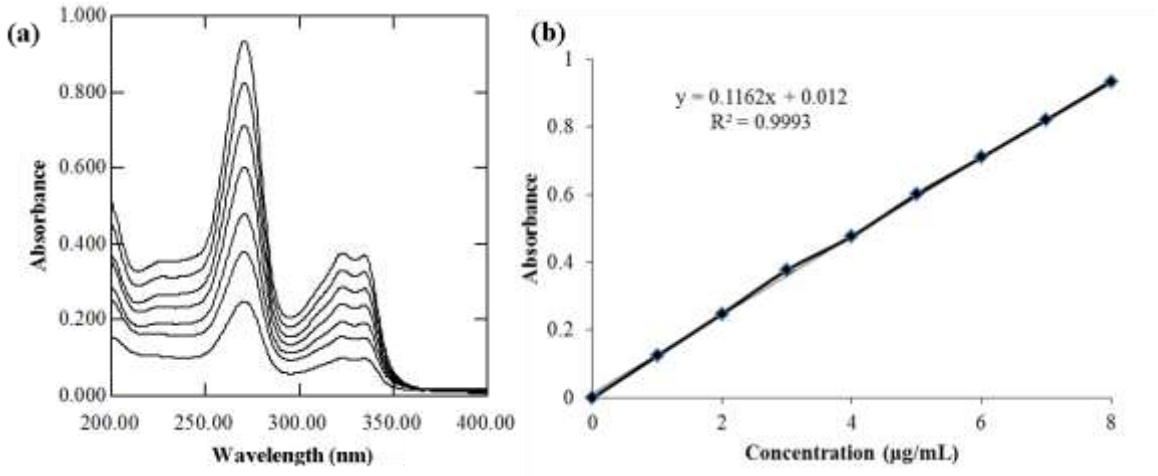

Figure 5.2: (a) Overlay spectra of a series of concentrations of ciprofloxacin hydrochloride and (b) its calibration curve in phosphate buffer (pH 7.4)

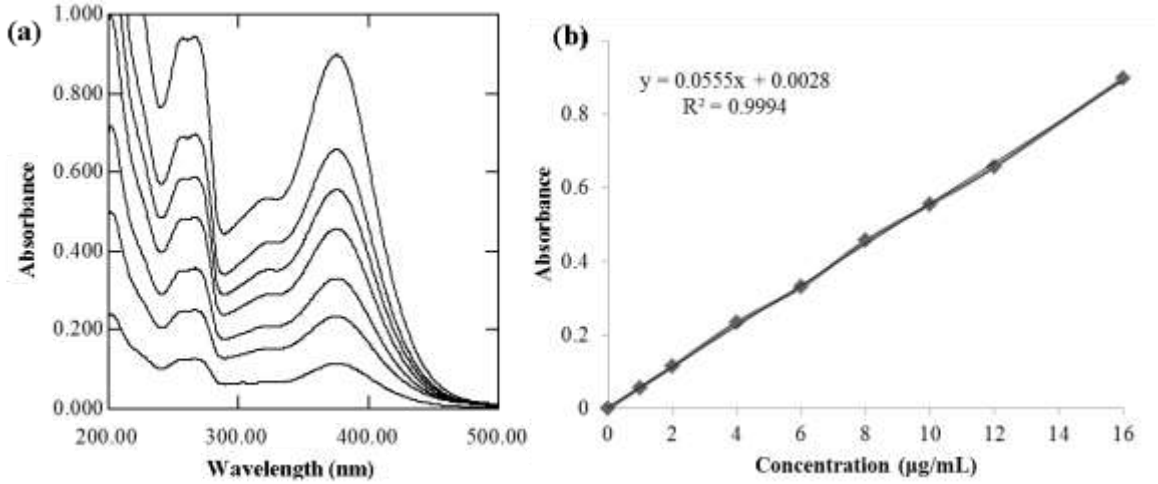

Figure 5.3: (a) Overlay spectra of a series of concentrations of quercetin and (b) its calibration curve in phosphate buffer (pH 7.4)

Table 5.1: λ_{max} value, concentration range, regression equation and coefficient, and molar absorptivity of ciprofloxacin hydrochloride and quercetin

Drug	λ_{max} Value (nm)	Concentration Range (µg/mL)	Regression Equation	Regression Coefficient (R^2)	Molar Absorptivity (Liter/mole/cm)
Ciprofloxacin Hydrochloride	271	1-8	y=0.1162x+0.012	0.9993	at 271 44210.68 at 370 809.1805
Quercetin	370	1-16	y=0.0555x+0.003	0.9994	at 271 17529.70 at 370 16774.11

5.1.2. Validation of developed method for the estimation of ciprofloxacin hydrochloride and quercetin by UV-Vis spectroscopy

Validation of the developed methods was performed as per the ICH guidelines. For exact estimation of CH and Que in a solution, the accuracy of developed method was performed by standard addition method and results were reported in terms of percentage recovery. The recovered drug (µg/mL) and percentage recovery at three different levels are shown in Table 5.2. The acceptance criterion for accuracy is mean value which should be within ±15% of the actual value [Bressolle et al. 1996, Shah et al. 1991]. The accuracy (%recovery) of the method was found to be 100±10% indicating the fair agreement between true and obtained values.

Table 5.2 Accuracy of developed method

Drug	Pre-analyzed Sample	Level of Recovery	Drug Added (µg/mL)	Drug Recovered* (µg/mL)	Recovery (%)
Ciprofloxacin Hydrochloride	8µg/mL	80%	6.4	6.530±0.125	102.0313
		100%	8	7.583±0.150	94.79167
		120%	9.6	9.883±0.110	102.9514
Quercetin	16µg/mL	80%	12.8	11.713±0.432	91.51042
		100%	16	16.903±0.736	105.6458
		120%	19.2	20.373±0.596	106.1111

*Values represent mean±SD (n=3).

The precision of the developed method was validated by re-analysing the three different concentrations of CH and Que in a solution on intra-day (0h, 12h and 24h) and inter-day (1st day, 2nd day and 3rd day) and results are reported in terms of % RSD (relative standard deviation) (Table 5.3). The percentage RSD not exceeding 2% is the acceptance criteria for precision [Jain et al. 2011, Khalid et al. 2015]. The RSD (%) value for both intra-day and

inter-day observation were within 2%, which indicated high precision and sensitivity of the developed method for CH and Que analysis.

Table 5.3: Intraday and inter day precision of developed method

Drug	Theoretical Drug Conc. (µg/mL)	Intraday Precision		Inter day Precision	
		Calculated Drug Conc. (µg/mL)*	RSD (%)	Calculated Drug Conc. (µg/mL)*	RSD (%)
Ciprofloxacin Hydrochloride	2	1.903±0.025	1.322	1.903±0.032	1.689
	6	5.883±0.060	1.025	5.853±0.055	0.941
	8	7.837±0.050	0.642	7.837±0.068	0.869
Quercetin	4	3.870±0.066	1.694	3.837±0.055	1.436
	8	7.810±0.050	0.64	7.790±0.040	0.513
	12	11.763±0.142	1.206	11.737±0.136	1.16

*Values represent mean±SD (n=3).

The sensitivity of measurement of CH and Que by the developed simultaneous equation method was estimated in terms of limit of detection (LoD) and limit of quantification (LoQ) and shown in Table 5.4. Obtained LOD and LOQ values indicate that drugs can be quantified accurately in microgram concentration range by UV-spectrophotometric method.

Table 5.4: Detection and quantification limit of drugs

Drug	Limit of Detection (LoD)	Limit of Quantification (LoQ)
Ciprofloxacin Hydrochloride	0.490µg/mL	1.486µg/mL
Quercetin	1.234µg/mL	3.740µg/mL

5.1.3. Solubility studies

Solubility of CH and Que was determined by shake-flask-method. The obtained solubility of CH and Que in phosphate buffer (pH 7.4) are summarized in Table 5.5.

Table 5.5: Solubility of ciprofloxacin hydrochloride and quercetin in phosphate buffer (pH 7.4)

Drug	Solubility (mg/mL)*
Ciprofloxacin Hydrochloride	0.161±0.014
Quercetin	0.065±0.011

*Values represent mean±SD (n=3).

Fabrication, *In-vitro*, and *In-vivo* Evaluations of Different Nanofibers Loaded with Ciprofloxacin Hydrochloride and Quercetin

In the present research work, three novel combinations of nanofibers were fabricated by electrospinning technique for the healing of a full thickness wound: (1) PCL based nanofibers loaded with ciprofloxacin hydrochloride and quercetin (PCL-CH-Que nanofibers); (2) PCL-GE based nanofibers loaded with ciprofloxacin hydrochloride and quercetin (PCL-GE-CH-Que nanofibers); (3) PLGA-GE based nanofibers loaded with ciprofloxacin hydrochloride and quercetin (PLGA-GE-CH-Que nanofibers). The fabricated nanofibers were extensively evaluated for different *in-vitro* as well as *in-vivo* characterizations. The study was divided into three parts as stated below:

5.2. Fabrication and Characterization of PCL Based Nanofibers Loaded with Ciprofloxacin Hydrochloride and Quercetin

PCL based nanofibers of different composition were successfully electrospun using acetic acid/formic acid solvent system, which is one of the most commonly used solvents composition for electrospinning. This combination (acetic acid : formic acid; 7:3 ratio) produced a solvent system of optimum conductivity, which resulted into stable Taylor

cone, continuous and homogenous nanofibers formation. Various properties of fabricated nanofibers such as morphology, average diameter (nm), membrane porosity (%) and entrapment efficiency (%) are displayed in Table 5.6.

Table 5.6: Morphology, porosity and entrapment efficiency of different PCL based nanofibers.

Sample	Fiber Morphology	Average Diameter (nm)*	Membrane Porosity (%)	Entrapment Efficiency (%)
PCL (8%)	Beaded nanofibers	60.35±20.48	80.35%	-
PCL (12%)	Bead-free, semi-continuous nanofibers	79.07±22.49	78.56%	-
PCL (12%) – CH (10%)	Bead-free, continuous, lateral fibrils	126.11±33.57	72.70%	CH: 91.56%
PCL (12%) – CH (10%) –Que (5%)	Bead-free, continuous, with a few lateral fibrils	101.59±29.18	69.36%	CH: 92.04% Que: 94.32%

*The data are expressed as mean±SD (n=100).

5.2.1. Morphological study

Effect of polymer concentration and drugs concentration on nanofibers diameter and morphology can be seen in Figure 5.4. At low polymer concentration (8% w/v) nanofibers with a thin diameter (60.35±20.48nm) and beaded structure was produced (Figure 5.4 (a)). The plausible reason is insufficient viscosity of electrospinning solution which experiences two instability during travel from the nozzle to collector. First one is higher bending instability which results into thin diameter nanofibers [Khan et al. 2016], another one is Rayleigh instability which results into a beaded structure [Rieger et al. 2013]. As the polymer concentration increased to provide sufficient viscosity, bead-free fiber with thick diameter (79.07±22.49nm) was obtained (Figure 5.4 (c)). The probable reason is sufficient viscosity solutions which provide higher resistance to the jet against bending instability and

Rayleigh instability. When CH was added, it results in more continuous nanofibers with little lateral fibrils (Figure 5.4 (e)). CH incorporation results into enhancing polarity of solution due to HCl salt. This additional charge increases the repulsive forces between adjacent charged molecule carried by jet and result into lateral fibrils [Reneker et al. 2000]. Very few lateral fibrils were observed in PCL-CH-Que nanofibers which might be due to dilution of charge by addition of Que (Figure 5.4(g)). No significant difference had been observed between the diameter of PCL-CH nanofibers (126.11±33.57 nm) and PCL-CH-Que nanofibers (101.59±29.18 nm).

Porosity of a nanofiber membrane becomes an important parameter, when it is intended to be used for skin reconstitution. The porous nature of nanofibers would be helpful for cellular infiltration and proliferation; exchange of exudates, gases, and nutrients across the wounded area. The ideal porosity of nanofiber membrane should usually be within the range of 60–90% [Chong et al. 2007]. The developed membranes possessed the optimum porosity (data shown in Table 5.6) with randomly oriented nanofibers, which closely mimic the natural ECM.

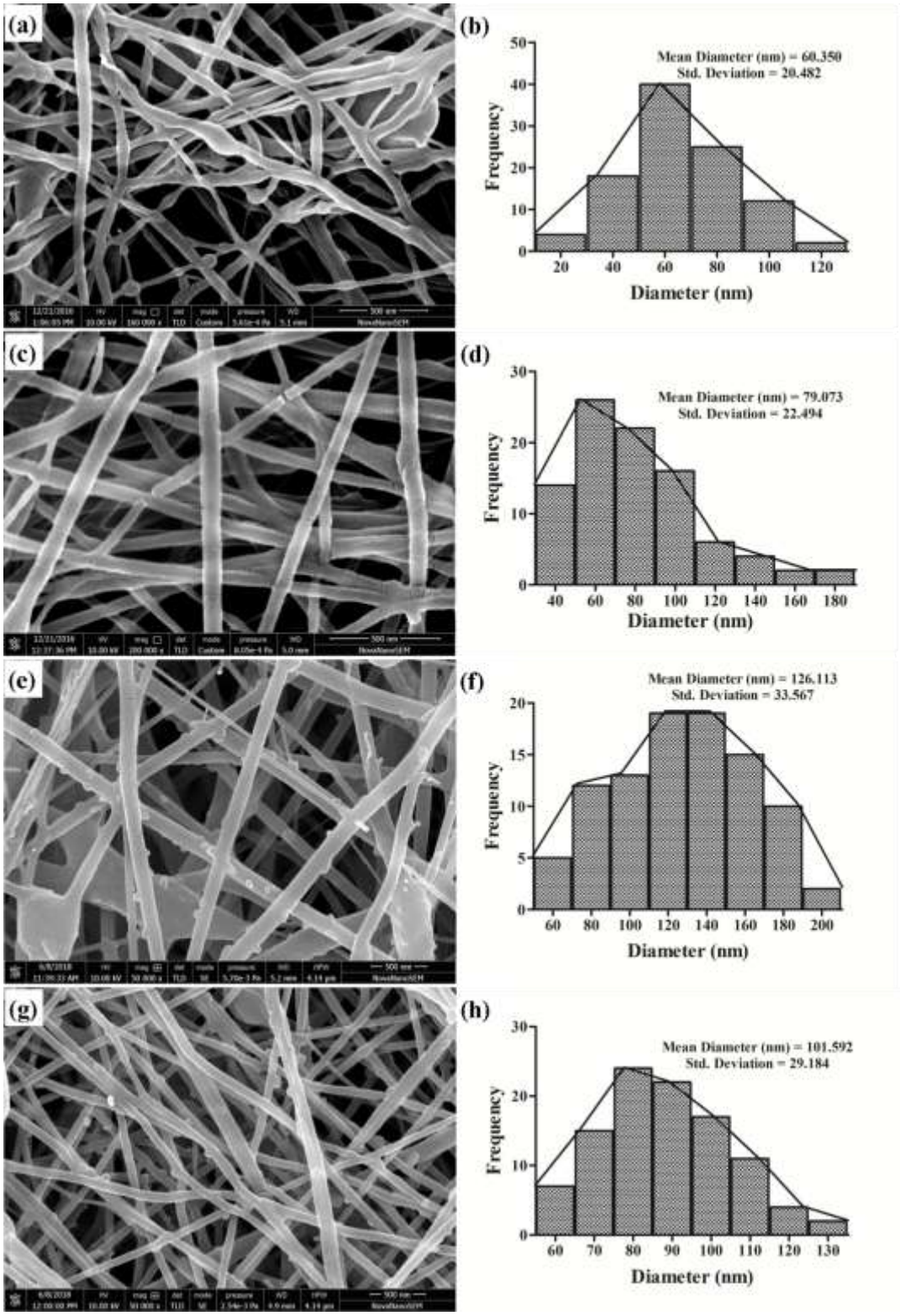

Figure 5.4: The HR-SEM micrograph of nanofibers and histogram of fiber diameter with respect to its distribution frequency: (a,b) PCL nanofibers (8% w/v), (c,d) PCL nanofibers (12% w/v), (e,f) PCL-CH nanofibers, and (g,h) PCL-CH-Que nanofibers. The data are expressed as mean±SD, n=100.

5.2.2. Solid-state characterizations

FT-IR spectroscopy was done to explore the possible chemical interaction between drugs and polymer, stability of drugs as well as effect of electrospinning on the functional groups of drugs present in the formulation [Gaonkar et al. 2017, Khan et al. 2017]. FTIR spectra of CH, Que, PCL-CH-Que nanofiber membrane are shown in Figure 5.5. Characteristic peaks of CH appeared at 1708.99 cm^{-1} (C=O stretching vibration of carboxylic acid), 1624.1 cm^{-1} (ketone C=O stretching vibration), 804.34 cm^{-1} (C-F stretching vibration) and between 3350-3550 cm^{-1} (O-H and N-H stretching vibration). Likewise, Que spectrum exhibited its characteristic peaks at 1664.62 cm^{-1} (aryl ketone C=O stretching vibration), 1383 cm^{-1} (O-H bending vibration of phenol functional group) and a broad peak around 3400 cm^{-1} correspond to stretching vibration of five O-H phenolic groups. FTIR spectra of fabricated nanofiber displayed diminished peaks (due to quite low amount of drugs in comparison to polymers amount) and peak masking by polymer's IR peaks. However, drugs-polymer interaction can be negated on the basis that the drugs were showing their characteristic λ_{max} values after getting released in dissolution media, and the formulation was capable to inhibit *S. aureus* growth on agar plate and scavenged the DPPH free radicals in the solution. Therefore, it can be concluded that the drugs and polymer were chemically compatible and electrospinning process did not adversely affect the functional groups of CH and Que.

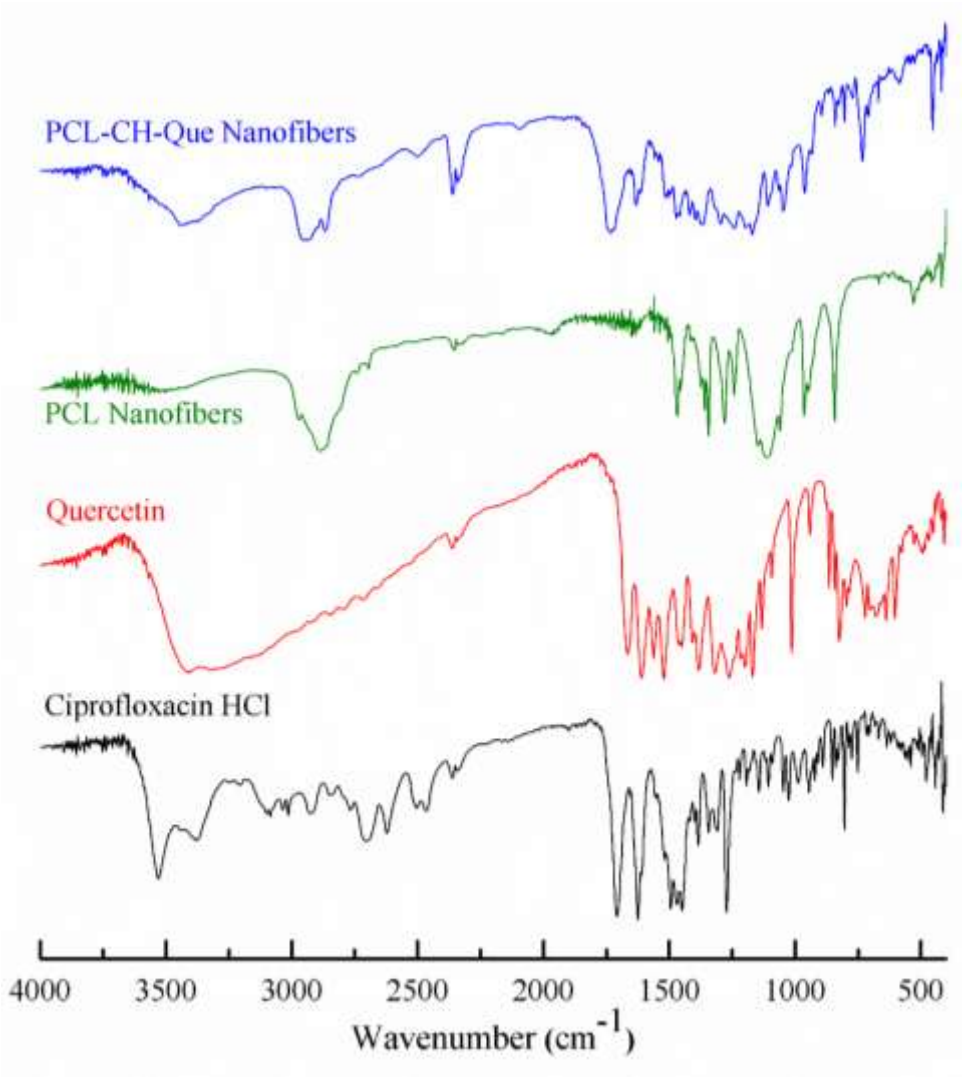

Figure 5.5: Chemical characterization of ciprofloxacin hydrochloride, quercetin, PCL nanofibers, and drugs loaded PCL-based nanofibers via FT-IR.

To determine the change in crystallinity of drugs encapsulated into nanofibers, XRD spectra of pure drugs, PCL, and PCL-CH-Que nanofibers were recorded (Figure 5.6). As reported earlier, CH spectra displayed its characteristic peak at 2θ of 8.2°, 9.04°, 19.3°, 24.72° and 26.48° which denotes its crystalline nature [Kataria et al. 2014]. The crystalline nature of Que was confirmed by distinct peaks at 10.74°, 12.42°, 27.34° [Qi et al. 2015]. Two diffraction peaks at 21.6 and 23.9 revealed the semi-crystalline nature of PCL [Xue et al. 2014]. The disappearance of diffraction peaks of drugs in the formulation elucidated that

a portion of drugs had been entrapped in the nanofibers and rest of the amount got aggregated on nanofibers surface in amorphous form, since rapid *in-situ* solidification didn't provide sufficient time for re-crystallization of drugs molecules on the surface. This finding was further confirmed by burst release of drug during *in-vitro* release studies.

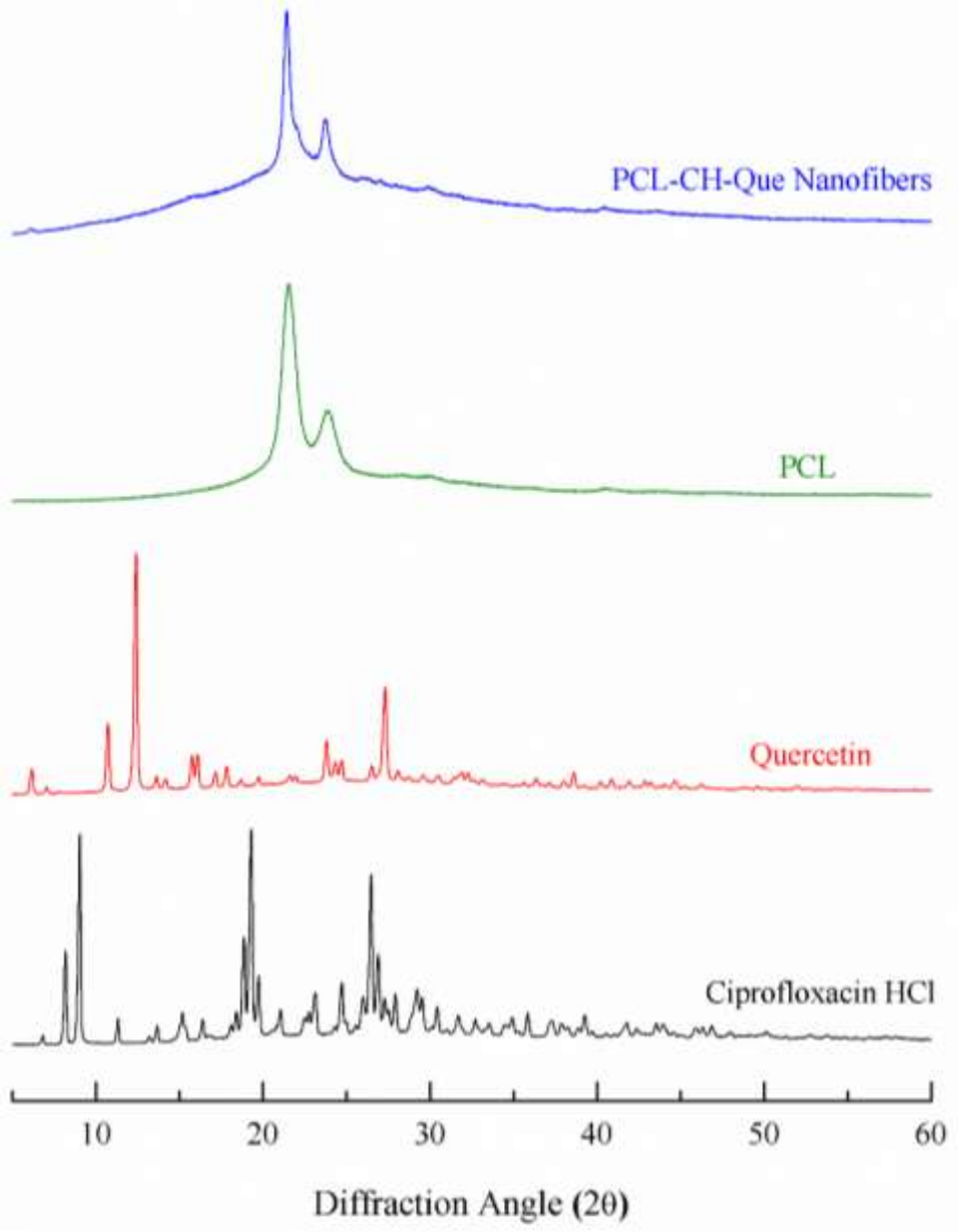

Figure 5.6: Overlay XRD spectra of ciprofloxacin hydrochloride, quercetin, PCL and drug loaded PCL-based nanofibers.

5.2.3. Contact angle of nanofiber membrane

Adhesion and proliferation of fibroblast on nanofiber membrane depends on its surface property. A hydrophilic surface augments the cell adhesion and proliferation while hydrophobic surface shows poor cell adhesion. The hydrophilicity of the nanofiber surface was examined by measuring the contact angle between a sessile drop of water and membrane surface. The average contact angle values for PCL was 100.1±2.285°, which was due to hydrophobic nature of PCL polymer. Mixing of drugs with polymer resulted into significantly ($p < 0.05$) lower contact angle value (80.73±2.656°), which might be due to hydrophilic nature of ciprofloxacin hydrochloride. The contact angle of PCL and PCL-CH-Que nanofibers did not change significantly till 2 min.

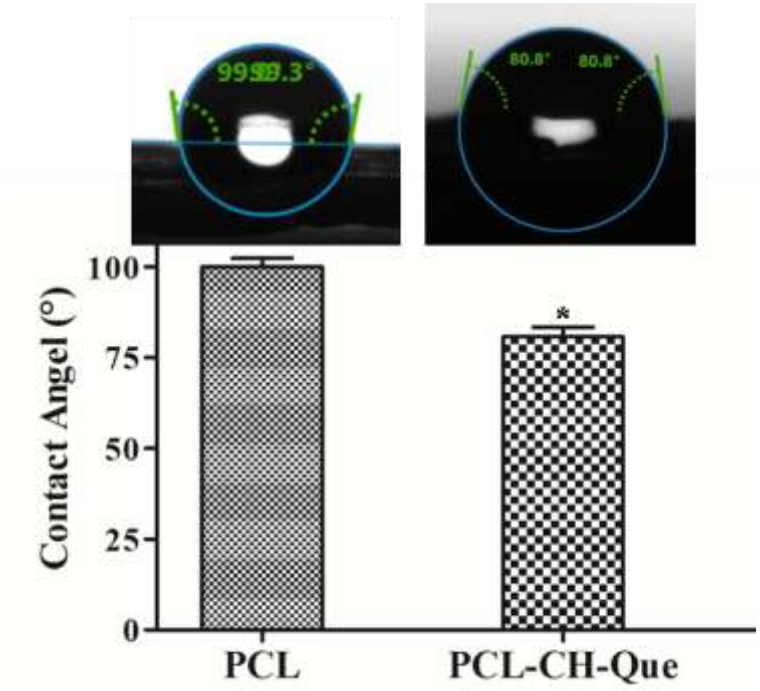

Figure 5.7: Water droplet profile and quantitative value of contact angle for PCL (100.1±2.285°) and PCL-CH-Que nanofiber (80.73±2.656°). The data are expressed as mean and vertical bar represents SEM (n=3). The data was analyzed by applying 'Unpaired t test' statics. [a]$p < 0.05$ vs PCL nanofibers.

5.2.4. Drug entrapment efficiency and *in-vitro* release study

Since only *in-situ* solidification of the polymer solution takes place in electrospinning, therefore, the entrapment efficiency of a nanofiber film should be almost 100%, under the consideration of complete miscibility of drugs and polymer, non-volatile nature of the drugs, and optimum concentration of the drugs. At higher concentration of the drugs, the encapsulation efficiency decreases, most likely due to the loss of excess drugs as the aggregate on the nanofiber surface, which escape encapsulation into the nanofibers. The fabricated nanofibers exhibited high entrapment efficiency of both drugs, (data shown in Table 5.6) which might be due to better miscibility of polymer and drug(s), and negligible loss of drug(s).

The *in-vitro* release profiles of PCL-CH-Que- nanofibers in phosphate buffer (pH7.4) are shown in Figure 5.8. The release of encapsulated drugs occurred in a biphasic manner, with an initial burst release followed by prolonged release. The initial burst release could be due to leaching of drug molecules located close to the surface of nanofiber membrane which was in immediate contact with dissolution media while the prolonged release might be due to diffusion of the drugs molecules that is lying deeper within the PCL nanofibers. Poor solubility of Que at pH7.4 might be the plausible reason for its low initial burst release (39.78% in 8h) and lower cumulative release (85.09% in 6days) in comparison to CH release as shown in Table 5.7. Since the fundamental purpose was to reduce the bacterial infection and attenuation of ROS generated during the early phase of wound healing, the burst release of CH and Que was desired and the same was observed in PCL-CH-Que nanofiber membrane.

Table 5.7: *In-vitro* drug release data of PCL based nanofiber membrane in phosphate buffer (pH 7.4)

Time (h)	Cumulative Percentage Drug Release	
	Ciprofloxacin Hydrochloride	Quercetin
0	0.00	0.00
0.5	27.60±3.23	18.79±2.41
1	36.93±4.02	25.96±1.99
3	41.98±3.82	31.79±2.03
5	45.21±5.30	35.91±2.85
8	49.98±2.39	39.78±3.01
10.33	53.82±4.02	43.80±2.67
25.33	69.30±5.56	55.31±4.52
33.33	75.79±5.24	60.97±4.68
50.33	85.18±4.60	69.16±5.67
57.08	88.71±3.55	73.41±3.91
73.33	94.92±5.02	78.88±4.67
96	96.79±4.68	83.09±3.96
120	97.99±3.46	84.54±3.10
144	98.98±2.61	85.09±2.89
156	98.99±3.45	85.39±4.34

The values are expressed as mean±SD (n=3).

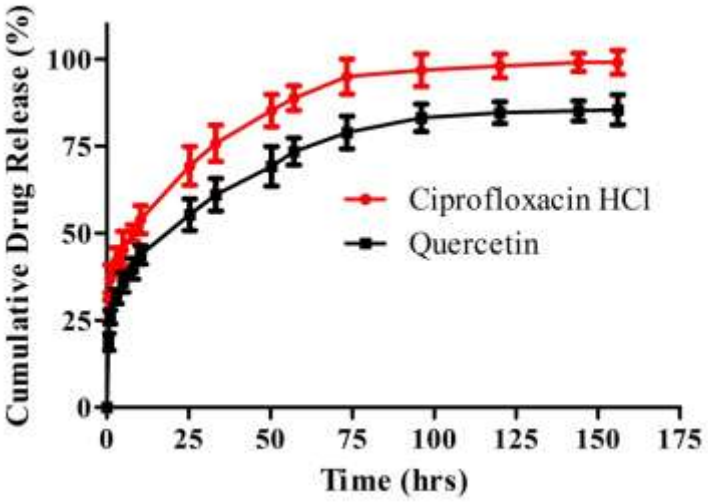

Figure 5.8: *In-vitro* cumulative drug release profiles of ciprofloxacin hydrochloride and quercetin loaded nanofibers in phosphate buffer (pH 7.4). The data are expressed as mean and vertical bar represents SD (n=3).

5.2.5. *In-vitro* antibacterial activity

The antimicrobial activity of fabricated nanofibers was tested against *S. aureus* by using film diffusion method and shown in Figure 5.9. Placebo nanofibers exhibit no antimicrobial property at all times as shown in Table 5.8. In contrast, PCL-CH and PCL-CH-Que nanofibers displayed initially broad inhibition zone due to burst release of antimicrobial, which narrowed down with time due to low and sustained release of antibiotic. PCL-CH-Que nanofibers exhibited a little wide inhibition zone than PCL-CH nanofibers, although no significant difference between PCL-CH and PCL-CH-Que nanofibers antimicrobial activity had been observed at any time. Therefore, it can be concluded that electrospun film was active enough to prevent microbial growth during the study period.

Table 5.8: Diameter of *S. aureus* inhibition zone on agar plate after incubation with different PCL based nanofiber membranes.

Time (days)	PCL Nanofibers	PCL-CH Nanofibers	PCL-CH-Que Nanofibers
1	0	32.13±2.50	33.28±1.80
3	0	27.04±3.22	29.11±2.57
5	0	26.03±2.54	28.89±3.00
7	0	26.01±3.55	26.98±3.10

The values are expressed as mean±SD (n=3).

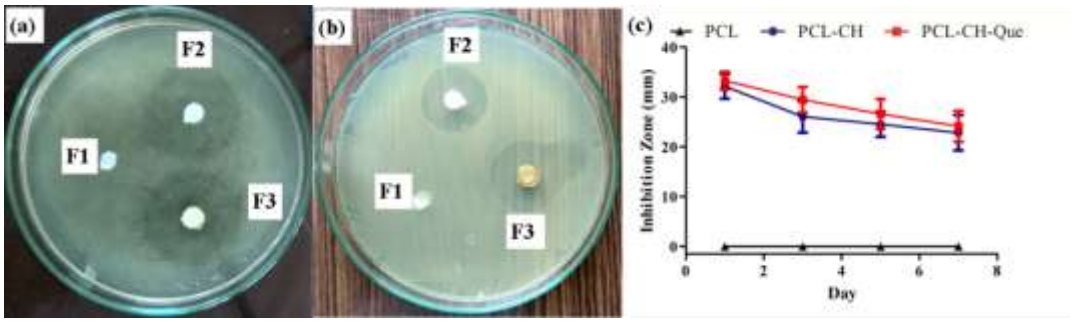

Figure 5.9: Antimicrobial activity of nanofiber membranes against *S. aureus*: (a) inhibition zone on day 1, (b) inhibition zone on day 3, (c) graphical illustration showing the relationship between diameters of inhibition zone (mm) vs incubation time (days). F_1, F_2, and F_3 represent the PCL, PCL-CH, and PCL-CH-Que nanofiber, respectively. The data are expressed as mean and vertical bar represents SD (n=3).

5.2.6. Free-radical scavenging efficiency of nanofibers

Antioxidant efficacy of the nanofiber film has been examined by DPPH assay and shown in Figure 5.10. The fundamental principle behind this assay is that DPPH is a stable free radical with maximum absorbance at 517nm and it changes its color from purple to yellow on accepting a hydrogen (H) or an electron from the antioxidant (like quercetin) and is reduced itself to $DPPH_2$. The color change is measured by UV-spectrophotometer at 517nm and utilized for quantification of antioxidant concentration in the solution [Mishra et al. 2012, Selvaraj and Fathima 2017]. It was found that PCL nanofibers and PCL-CH nanofibers also exhibited slight antioxidant activity, 5.75%, and 12.67% respectively, which might be due to terminal hydroxyl group in PCL and hydroxyl group in ciprofloxacin. PCL-CH-Que nanofibers exhibited quite significant ($p<0.001$) anti-oxidant property (40.13%) in comparison to PCL and PCL-CH nanofibers, which was attributed to phenolic groups in quercetin.

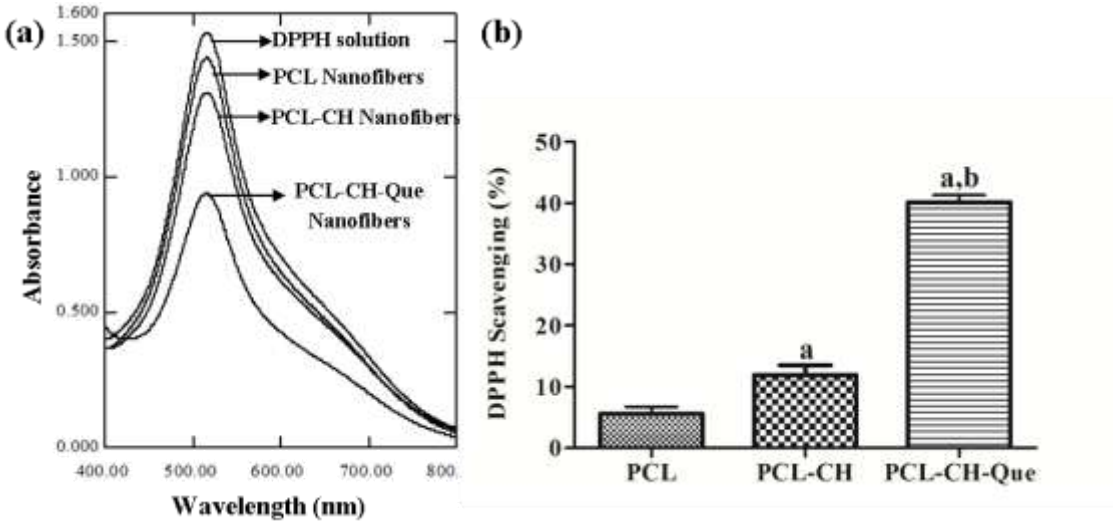

Figure 5.10: Free radical scavenging efficacies of the PCL, PCL-CH, and PCL-CH-Que nanofiber after 0.5h incubation with DPPH solution: (a) UV-Vis spectra; (b) histogram representing DPPH attenuation efficiencies of different nanofiber membrane. The data are expressed as mean and vertical bar represents SD (n=3). $^{a}p < 0.05$ vs PCL nanofibers, $^{b}p<0.05$ vs PCL-CH nanofibers.

5.2.7. Biocompatibility study

5.2.7.1. Hemocompatibility assessment of nanofiber membrane

Hemocompatibility of a nanofiber membrane proposed to be used in wound area is a vital requirement to maintain the integrity and functionality of RBCs in newly formed blood capillaries else it may cause some serious concern like thrombosis. Accordingly, hemocompatibility of nanofiber Film was evaluated by measuring the hemolytic property on human RBCs. The extent of RBCs hemolysis by electrospun nanofibers are shown in Figure 5.11. It was observed that hemolysis caused by all three types of nanofiber membrane was under acceptance limit i.e., <5%, as stated by Haghjooy Javanmard et al., [Haghjooy Javanmard et al. 2016]. The placebo nanofibers (PCL nanofiber) lysed 4.20±0.23% RBCs which might be due to high surface roughness of the film, while PCL-CH-Que caused significantly ($p<0.05$) low hemolysis in comparison to PCL and PCL-CH nanofiber which might be due to protective action of quercetin against lipid peroxidation of unsaturated fatty acid and thiol group (-SH) in RBCs membrane.

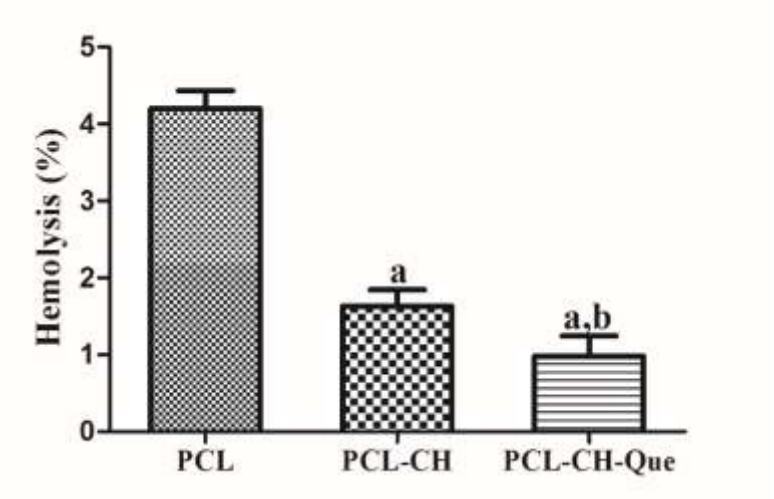

Figure 5.11: *In-vitro* hemocompatibility of PCL, PCL-CH and PCL-CH-Que nanofibers. The data are expressed as mean and vertical bar represents SD (n=3). $^{a}p < 0.05$ vs PCL nanofibers, $^{b}p < 0.05$ vs PCL-CH nanofibers.

5.2.7.2. Cytocompatibility assessment of nanofiber membrane

The Viability of fibroblast cell lines on 24h, 48h, and 72h was examined through MTT assay and shown in Figure 5.12. It was observed that the cell lines proliferated well in all aliquots throughout the study period, which confirm the nontoxic nature of nanofibers. At the end of each time point, cell lines treated with PCL-CH-Que nanofiber's aliquot showed significant ($p<0.05$) proliferation, which might be due to quercetin, a flavonoid. Flavonoids are found to improve the fibroblast proliferation and collagen synthesis, as reported by Selvaraj and Fathima, 2017.

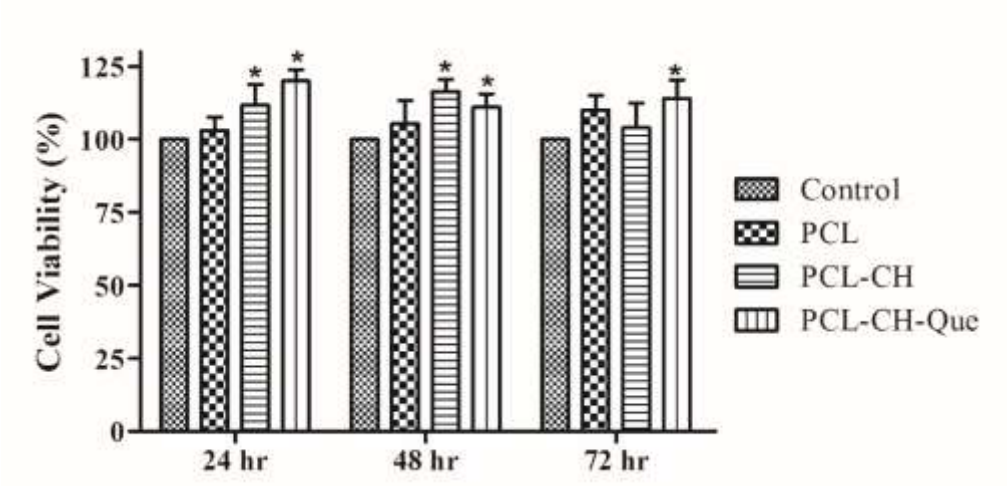

Figure 5.12: Viability of Swiss albino 3T6 fibroblast cells on nanofibrous scaffolds after different culture times. The data are expressed as mean and vertical bar represents SD (n=3). *p < 0.05 vs control. A cell suspension cultured into a well without any scaffold was considered as control.

5.2.8. Pilot study- wound healing efficiency of PCL-CH nanofiber membrane in comparison to CIPLOX cream

All the treated groups' animals did not show any post-operative side effects like sepsis, fluid retention, etc. throughout the treatment period. The representative images of healing wounds and the quantitative value of the healed area are shown in Figure 5.13. The CH

loaded nanofibers treated group shows significantly higher ($p < 0.05$) healing than gauze and CIPLOX treated group, which might be due to dual effect provided by PCL-CH nanofiber membrane, i.e. ECM mimicking architecture for cell proliferation and sustained release of antimicrobial for inhibiting bacterial infiltration. Owing to antibacterial property, the CIPLOX cream treated group achieved significantly higher ($p < 0.05$) healing in comparison to gauze treatment. This comparative result supports the significantly higher healing efficiency of ciprofloxacin hydrochloride loaded nanofibers and further exploration of healing effect of other medicament such as quercetin, an antioxidant.

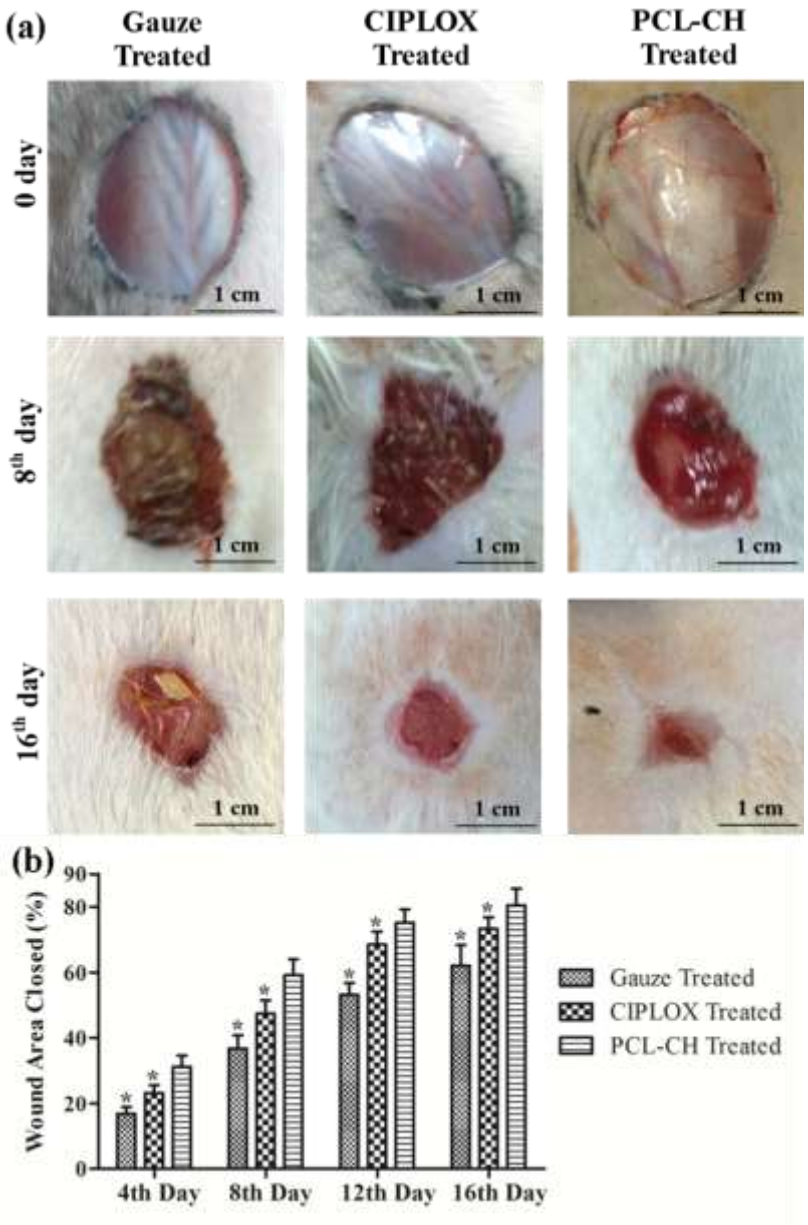

Figure 5.13: Effect of formulations for the healing of full thickness wound: (a)representative images of wound healing on day 8 and 16, (b) percentage of wound area closed following treatment with gauze, CIPLOX cream and PCL-CH nanofibers on day 4, 8, 12 and 16. The data are expressed as mean and vertical bar represents SD (n=3). *$p<0.05$ vs gauze treated.

5.2.9. *In-vivo* wound healing study

It can be observed from Figure 5.14 that among all treatment groups, PCL-CH-Que nanofibers treated group exhibited significantly high wound healing property at all the time

points. At the end of 4thday, PCL-CH-Que treated group displayed significant ($p<0.05$) healing (43.98%) in comparison to PCL-CH treated group (30.56%), which might be due to effective attenuation of ROS during inflammatory phase by burst released of quercetin.

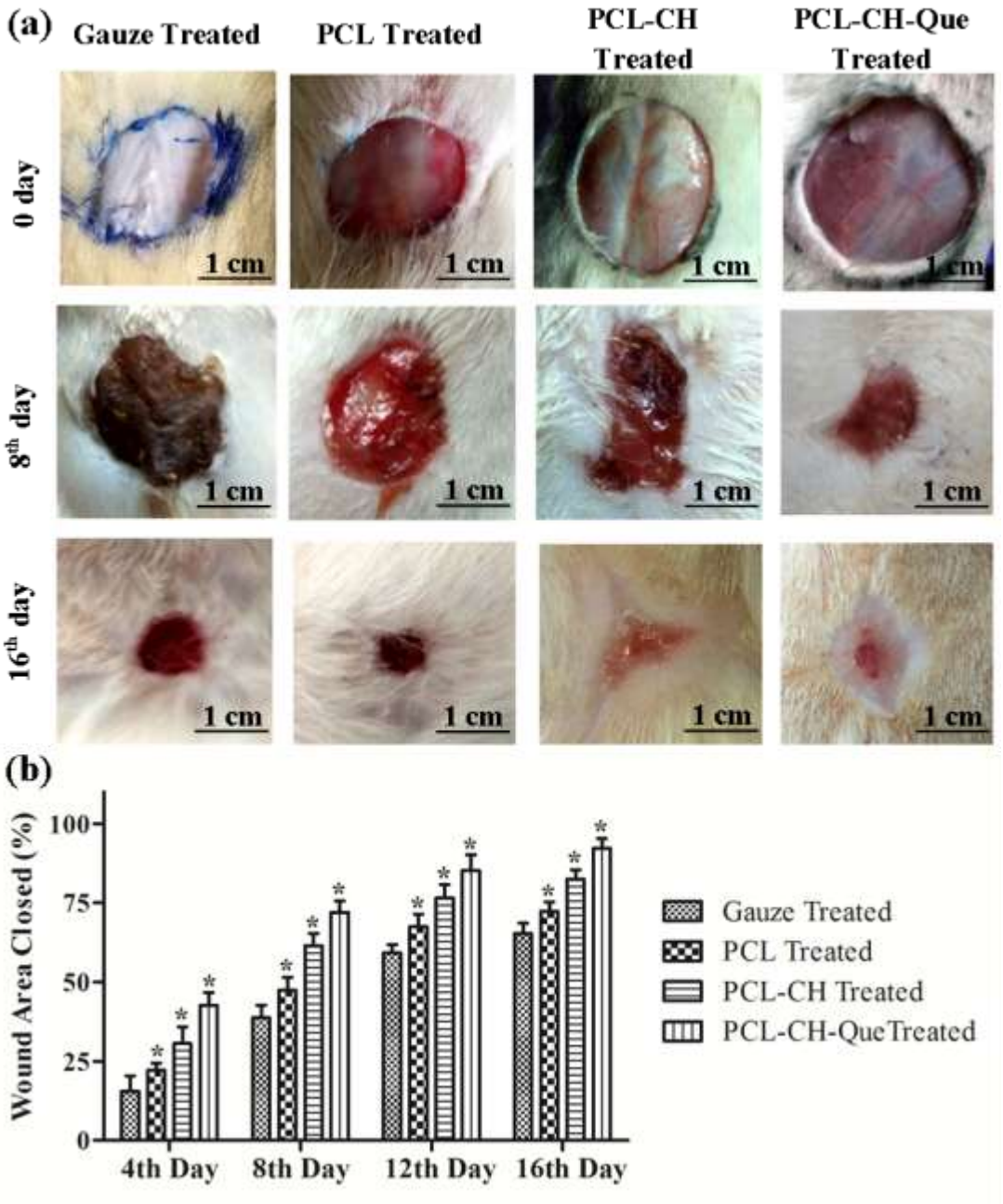

Figure 5.14: Effect of nanofibers for the healing of full thickness wound: (a) representative images of wound healing on day 8 and 16, (b) percentage of wound area closed following treatment with gauze, PCL, PCL-CH and PCL-CH-Que nanofibers on day 4, 8, 12 and 16. The data are expressed as mean and vertical bar represents SD (n=3). *$p < 0.05$ vs gauze treated.

Throughout the study period, PCL-CH and PCL-CH-Que group maintained a significant ($p<0.05$) wound healing efficiency with respect to gauze and PCL nanofibers treated group. Antimicrobial and antioxidant property of nanofibers might have reduced microbial infection, ROS level and prevented the oxidative damage of fibroblast, thereby improving the collagen synthesis and wound healing potential.

5.2.9.1. Histological examination of granulation tissues

The histological sections of H&E stained skin of gauze treated and nanofibers treated groups on day 8 and 16 are shown in Figure 5.15. On day 8, underplaying layers of granulated tissue of gauze treated group was infiltrated with inflammatory cells like neutrophils and basophils. Wounds in PCL nanofibers treated group displayed the granulation tissue with fewer fibroblasts along with neutrophils and macrophages.

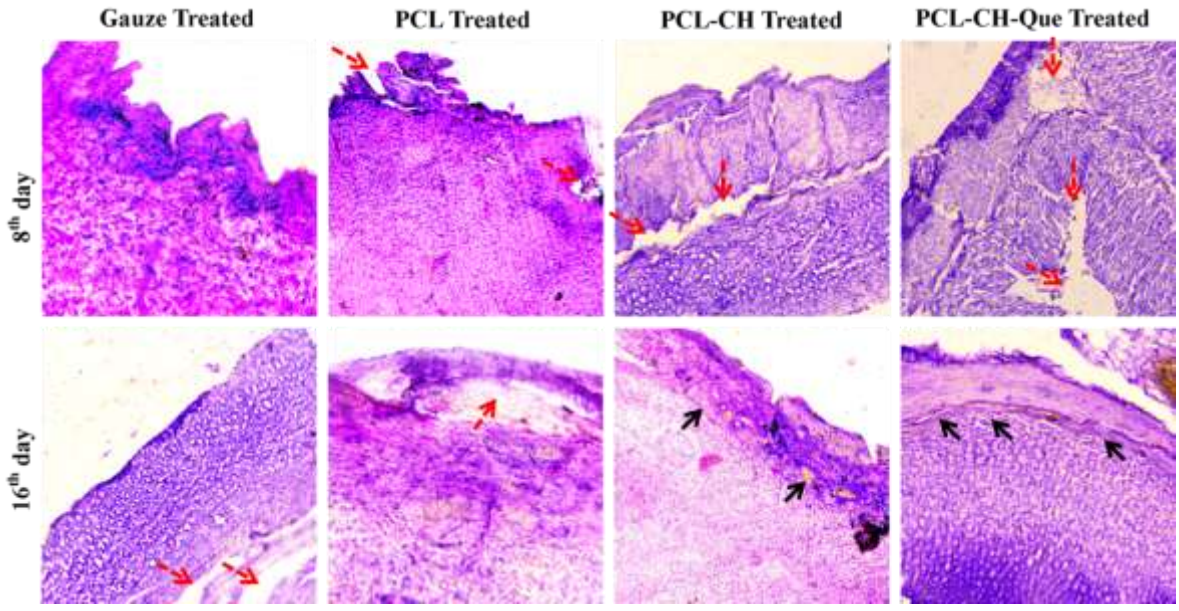

Figure 5.15: Haematoxylin−eosin stained slice showing histological changes in granulation tissue of gauze, PCL, PCL-CH and PCL-CH-Que nanofibers treated groups on day 8 and 16. Optical magnification was 10X. The black color arrow indicates growth of dermis and epidermis layer while red color arrow indicates lack of collagen synthesis in the dermis region.

Groups treated with PCL-CH and PCL-CH-Que-nanofibers demonstrated moderate amount of fibroblast as compared to the other groups, which confirm the accelerated wound healing. Inflammatory response is very low in PCL-CH-Que treated group, establishing the anti-oxidant activity of quercetin. All four groups displayed moderate amount of blood capillaries.

On day16, gauze treated group shows incomplete re-epithelialization and PCL nanofibers treated group showed moderate epithelialization along with thin epidermis. Both groups displayed poor collagen synthesis as white spaces in dermis region. On the other side, PCL-CH and PCL-CH-Que nanofibers treated groups exhibited well developed epidermis and dermis layer along with keratinocyte infiltration and good collagen deposition in epidermis and dermis layer respectively.

5.2.9.2. Antioxidant enzyme activity in granulation tissues

In the excision wound model, the inflammatory phase generally spans for 1-4days, during which ROS generated beyond the physiological need [Nafiu and Rahman 2015]. During this phase, endogenous anti-oxidants become insufficient to attenuate this excess ROS. Even exogenous anti-oxidant (like Quercetin) did not restore the activity of endogenous enzymes significantly in the first week of study, which could be observed in Figure 5.16 (a) & (b). At the end of first week none of the groups exhibited significant improvement in the amount of SOD and catalase. Although, PCL-CH-Que nanofibers treated animals demonstrated improvement in anti-oxidants level in comparison to other groups, which could be due to potential anti-oxidant property of quercetin, but still a significant difference ($p < 0.05$) was observed with respect to control. During proliferative phase (5-11days), only a small amount of ROS were generated which could be attenuated by collective effect

of extracellular and intracellular anti-oxidants. Therefore, during those phases extracellular antioxidant helped in restoration of SOD and catalase level, as observed at the end 16th day. Quercetin loaded nanofibers group had achieved SOD and catalase level very close to control ($p > 0.05$) and meanwhile it had also achieved a significant improvement in antioxidants level when compared with rest treated groups.

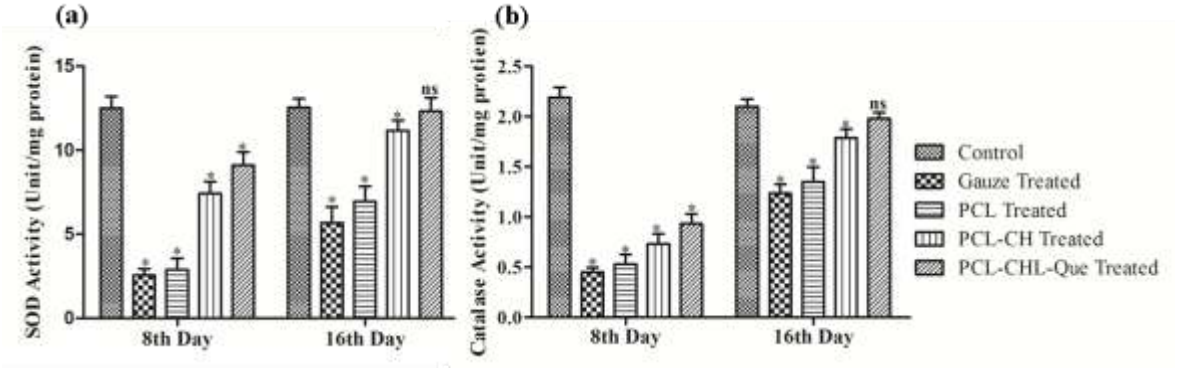

Figure 5.16: Biochemical assessment of granulation tissue harvested from wound area in terms of (a) SOD and (b) catalase activity on day 8th and 16th. $^{*}p<0.05$ and $^{ns}p>0.05$ versus gauze treated group. The data are expressed as mean and vertical bar represents SD (n=3). Control is an unwounded group.

5.2.8.3. Hydroxyproline content in granulation tissues

Granulation tissue is mainly constituted of collagen fiber, fibroblast and newly developed blood vessel. Collagen fiber is composed of 13-14% hydroxyproline in addition to other amino acid. Hence, hydroxyproline level has been used as biochemical index for collagen content. The content of hydroxyproline or collagen fiber indicates activity of proliferating fibroblast and physical strength of regenerating tissue. On the 8th day, all groups demonstrated insignificant improvement in comparison with control, although PCL-CH-nanofibers and PCL-CH-Que nanofibers treated groups displayed significant improvement ($p<0.05$) in comparison to rest two groups (Figure 5.17). This increment could be attributed to pro-wound healing environment provided by nanofibers. On the 16th day, only

PCL-CH-Que nanofibers treated group showed significant increase in hydroxyproline level in respect to other groups. Although hydroxyproline level was higher in PCL-CH nanofibers treated group than in the gauze and PCL nanofibers treated group, but no significant difference could be achieved between PCL-CH nanofibers treated group and control. On both time points, PCL-CH-Que nanofibers treated animals exhibited significant ($p<0.05$) improvement in wound healing in respect of PCL-CH nanofibers treated group, which could be due to neutralization of reactive oxygen species and subsequently better collagenesis.

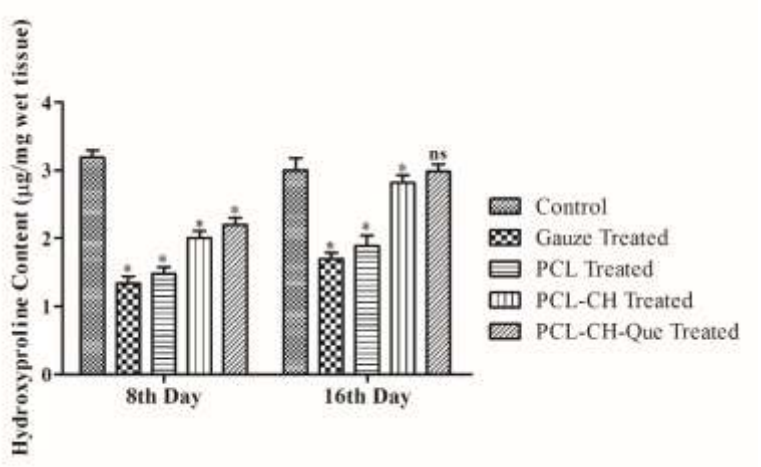

Figure 5.17: Effect of different nanofibers on hydroxyproline content in granulation tissue of rats on day 8 and 16 post-wounding. The data are expressed as mean and vertical bar represents SD (n=3). *$p<0.05$ vs Conrol Group, and $^{ns}p>0.05$ vs Control Group (unwounded).

Although, PCL is a widely studied synthetic polymer for electrospinning due to wide range of biological and chemical compatibility, mechanical strength and comparatively low cost (440744-500G: INR 21,974.57), however, hydrophobic nature, low biodegradation rate and absence of cell recognition site in PCL chain results into inefficient attachment of scaffold at wound site, partial degradation and assimilation of nanofibers during the course of healing, and incomplete closure of wound, as observed in above study. Further, slow

degradation of PCL scaffold in phosphate buffer (pH 7.4) took six days to release 98.98±2.61% ciprofloxacin HCl and 85.09±2.89% quercetin, which was ineffective to heal a chronic wound with severe microbial infiltration. Therefore, the blending of PCL with gelatin was proposed to obtain a scaffold with optimum hydrophilicity, biodegradation rate, and mechanical strength, as done by other researchers [Chong et al. 2007, Ghasemi-Mobarakeh et al. 2008, Ramalingam et al. 2019, Xue et al. 2014]. Gelatin (GE) is a hydrophilic biopolymer obtained from partial hydrolysis of collagen, the principal extracellular matrix building protein [Dulnik et al. 2016, Ghasemi-Mobarakeh et al. 2008]. Gelatin also contains cell-recognition site (Arg-Gly-Asp amino acid sequences), which is recognized by integrins and thus aids in cell attachment and it's spreading.

5.3. Fabrication and Characterization of PCL-GE Based Nanofibers Loaded with Ciprofloxacin Hydrochloride and Quercetin

PCL-GE based nanofibers of different composition were fabricated successfully using hexafluoro-2-propanol (HFIP) solvent. HFIP is most commonly used solvent for biopolymers by virtue of strong hydrogen-bonding properties and ability to break hydrophobic interactions [Nguyen et al. 2012, Zhang et al. 2010]. Moreover, boiling point of HFIP is quite low (60 °C), therefore, it volatilizes very quickly while electrospinning and also from the resulting nanofibers [Bide et al. 2010]. Various properties of fabricated nanofibers such as morphology, average diameter (nm), membrane porosity (%) and entrapment efficiency (%) are shown in Table 5.9.

Table 5.9: Morphology, porosity and entrapment efficiency of different PCL-GE based nanofibers.

Sample	Fiber Morphology	Mean Diameter (nm)*	Membrane Porosity (%)	Entrapment Efficiency (%)
PCL	Thin nanofibers with random beads	86.184±20.984	69.02	-
PCL-GE	Thick nanofibers with rough surface	234.172±98.234	73.98	-
PCL-GE-CH	Smooth nanofibers with frequent fibrils	518.148±167.894	74.31	CH = 89.02
PCL-GE-CH-Que	Smooth nanofibers with fewer fibrils and uniform size distribution	725.943±201.965	81.79	CH = 87.31 Que = 90.10

The values are expressed as mean ± SD, *n = 100

5.3.1. Morphology of electrospun nanofibers

Due to the sol-gel transition of gelatinous protein and the immiscibility of gelatin and PCL at isoelectric point, the mixed solution of gelatin/HFIP and PCL/HFIP became cloudy and slowly separates into two layers during electrospinning, which resulted into defective fiber morphology. When a little amount of glacial acetic acid was added to the opaque solution, the pH of the solution reduced from the isoelectric point of gelatin, which resulted into complete miscibility of gelatin and PCL, and homogenous electrospinning [Anjum et al. 2017, Xue et al. 2014].

The HR-SEM micrographs and corresponding histogram of nanofibers diameter are shown in Figure 5.18. The micrograph images demonstrate a randomly oriented, beadles and uniform structure. The mean diameter of PCL nanofiber membrane was found to be 86.184±20.984 nm. After blending the gelatin with PCL, the diameter of nanofibers increased significantly (234.172±98.234 nm) and was attributed to increase in viscosity of the solution [Anjum et al. 2017, Norouzi et al. 2015]. Further incorporation of drugs in

PCL-GE matrix resulted into nanofibers with increased average diameter, smooth surface and more uniform size distribution.

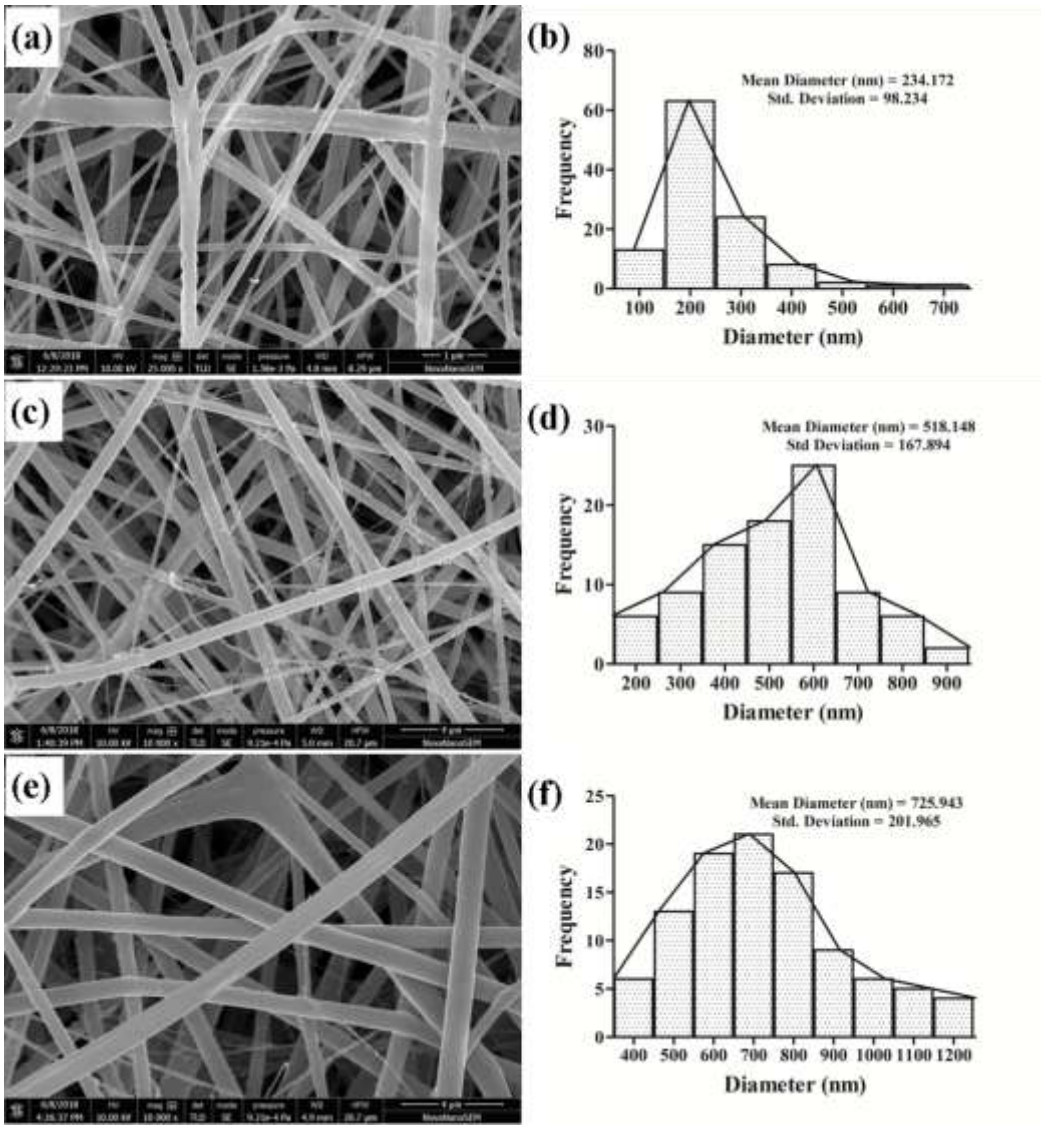

Figure 5.18: The HR-SEM micrograph of nanofibers and histogram of fiber diameter with respect to its distribution frequency: (a,b) PCL-GE nanofibers (1:1), (c,d) PCL-GE-CH nanofibers, and (e,f) PCL-GE-CH-Que nanofibers. The data are expressed as mean±SD, n=100.

The porosity of tissue-engineered nanofibers becomes a vital parameter especially when its application is anticipated for skin regeneration. The optimum porosity of the nanofiber membrane would be useful for cellular ingrowth and proliferation, infiltration of nutrients,

gases and exudates across the membrane. Generally, the ideal porosity of a nanofiber membrane for skin regeneration should be within 60-90% range [Chong et al. 2007]. The porosities of fabricated nanofibers were within this range (Table 5.9), ensuring sufficient exchange of nutrient and gas.

5.3.2. Solid-state characterizations

FT-IR spectroscopy was conducted to investigate any probable drugs and polymer interactions, drug stability and the effect of electrospinning on the functional groups of drugs in the formulation [Gaonkar et al. 2017, Khan et al. 2017]. FTIR spectra of ciprofloxacin hydrochloride and quercetin are shown in Figure 5.19. Ciprofloxacin hydrochloride showed its characteristic peak at 1624.11 cm^{-1} for ketone C=O stretching vibration, 1708.99 cm^{-1} for carboxylic acid C=O stretching vibration, 804.34 cm^{-1} for C-F stretching vibration and a broad shoulder for N-H and O-H stretching vibration (between 3350-3550 cm^{-1}). Similarly, major characteristic peak of quercetin appeared at 1383 cm^{-1} for O-H bending vibration of phenol functional group, 1664.62 cm^{-1} for aryl ketone C=O stretching vibration and a broad peak around 3400 cm^{-1} correspond to stretching vibration of five O-H phenolic groups. FTIR spectra of drug loaded nanofibers showed typical ciprofloxacin and quercetin peaks of weak intensity owing to very low amount of drugs and masking of some peaks by polymers' peak. Since drug loaded nanofibers was releasing the drug in dissolution media, attenuating the DPPH free radicals in methanol solution, and inhibiting microbial growth on agar plate, therefore, drugs-polymers interaction and change of drugs chemical nature could be ruled-out. It can, therefore, be concluded that drugs and polymers are chemically compatible and can be electrospun.

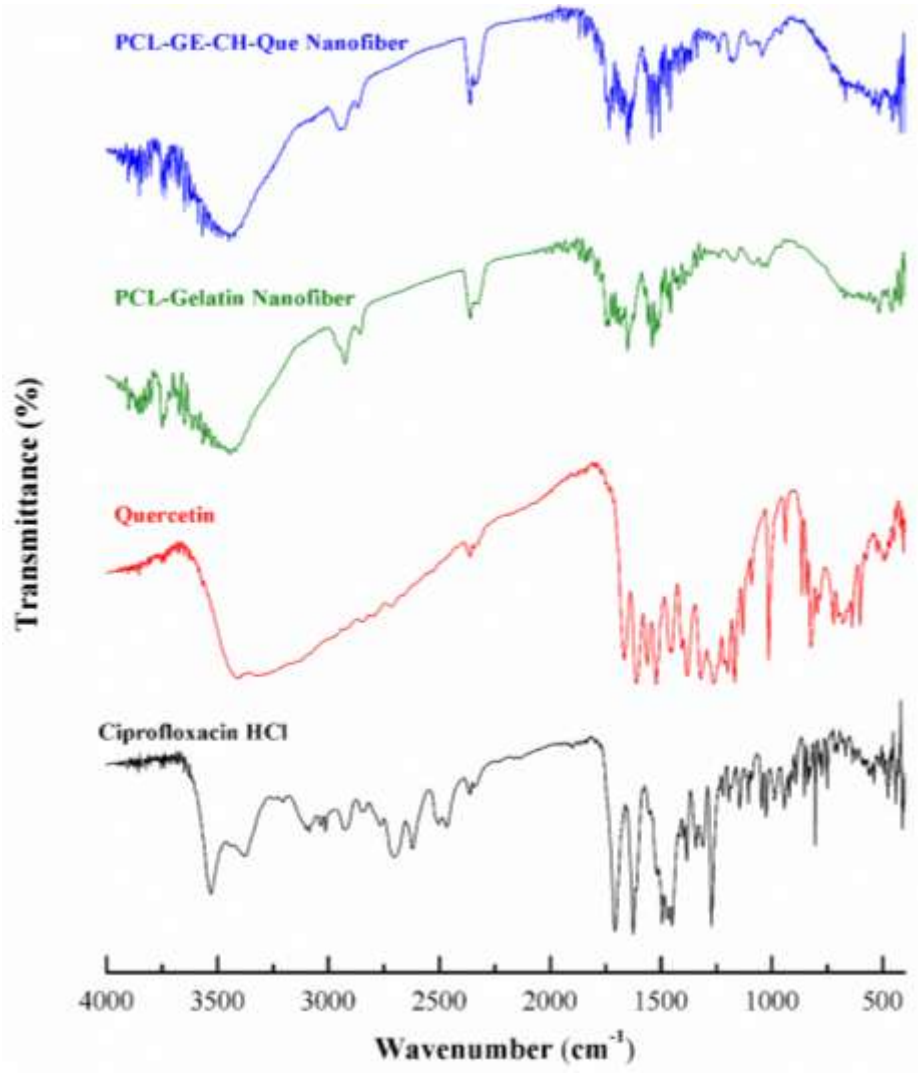

Figure 5.19: Chemical characterization of ciprofloxacin hydrochloride, quercetin, PCL-GE nanofibers and drug loaded PCL-GE based nanofibers via FT-IR.

XRD patterns of ciprofloxacin hydrochloride, quercetin, PCL, gelatin and fabricated nanofibers are shown in Figure 5.20. Ciprofloxacin hydrochloride spectra exhibited sharp diffraction peak at 8.2°, 9.04°, 19.3°, 24.72° and 26.48° in 2θ scale [Kataria et al. 2014], which signifies the crystalline nature of drug. Likewise, few distinct sharp peaks at 10.74°, 12.42°, 27.34° established the crystalline nature of quercetin [Qi et al. 2015]. Two diffraction peaks situated at 23.9° and 21.6° attributed to semi-crystalline nature of PCL [Xue et al. 2014]. Absence of any sharp peak in gelatin spectra denoted its amorphous

nature. In contrast, absence of characteristic peaks of drugs in PCL-GE-CH-Que spectra denotes that a portion of drugs had been entrapped in the nanofibers and rest of the amount got aggregated on nanofiber surface in amorphous form, since rapid in-situ solidification didn't provide sufficient time for re-crystallization of drugs molecules on the surface.

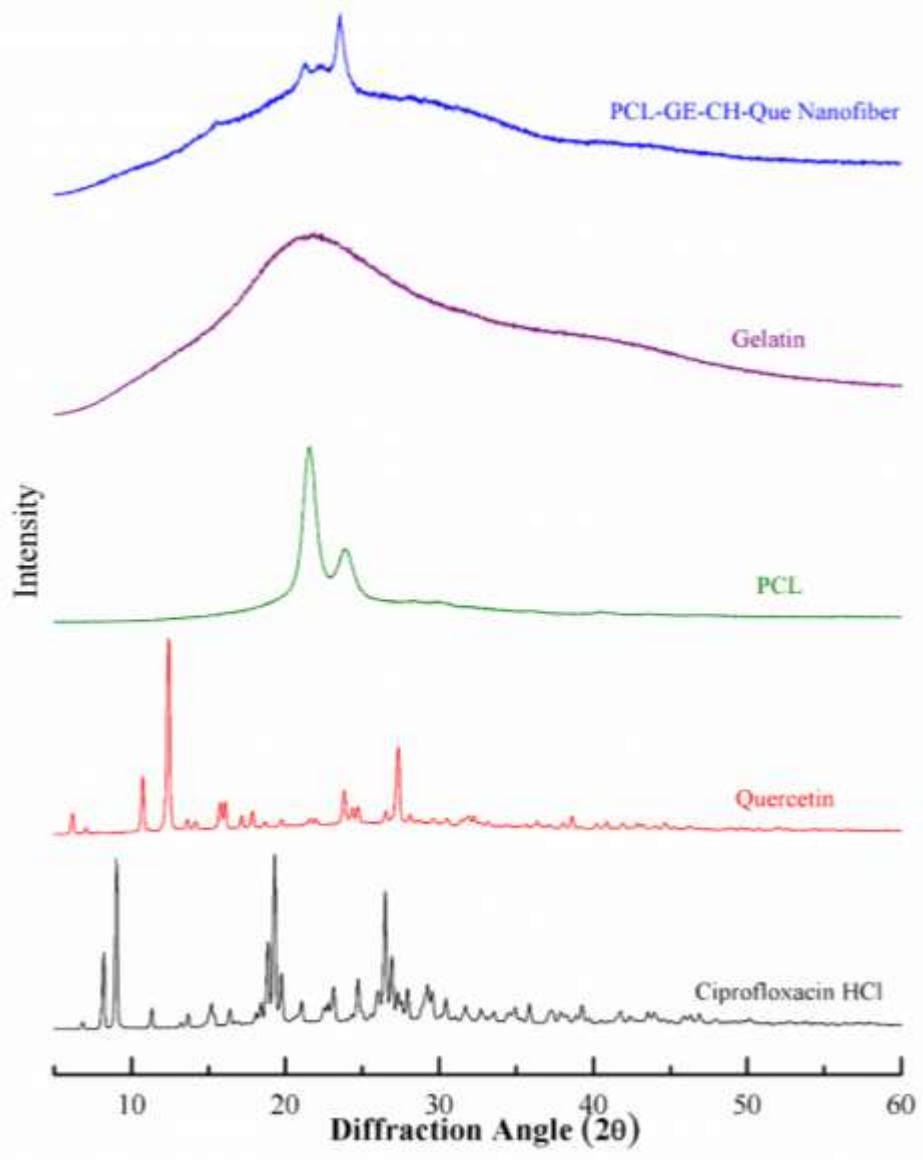

Figure 5.20: Overlay XRD spectra of ciprofloxacin hydrochloride, quercetin, PCL, gelatin and drug loaded PCL-GE based nanofibers.

5.3.3. Contact angle of nanofiber membrane

Contact angle represents the hydrophilicity of the surface which in turn affects the fibroblast adhesion and its proliferation on nanofibers. Despite having desirable biocompatible property, a PCL nanofiber suffers from severe hydrophobicity. Therefore, the effect of gelatin on hydrophobicity was evaluated and shown in Figure 5.21. It was found that gelatin reduced the contact angle very effectively, which was due to the hydrophilic nature of the protein. Further, the addition of ciprofloxacin hydrochloride also reduced the contact angle. The average contact angle value for PCL, PCL-GE, and PCL-GE-CH-Que nanofibers was 100.1±3.16°, 55.5±2.10°, and 48.8±2.95°, respectively. The contact angle of PCL-GE and PCL-GE-CH-Que nanofibers reached to 0° within the 30s, while that of PCL nanofibers did not change significantly till 2 min.

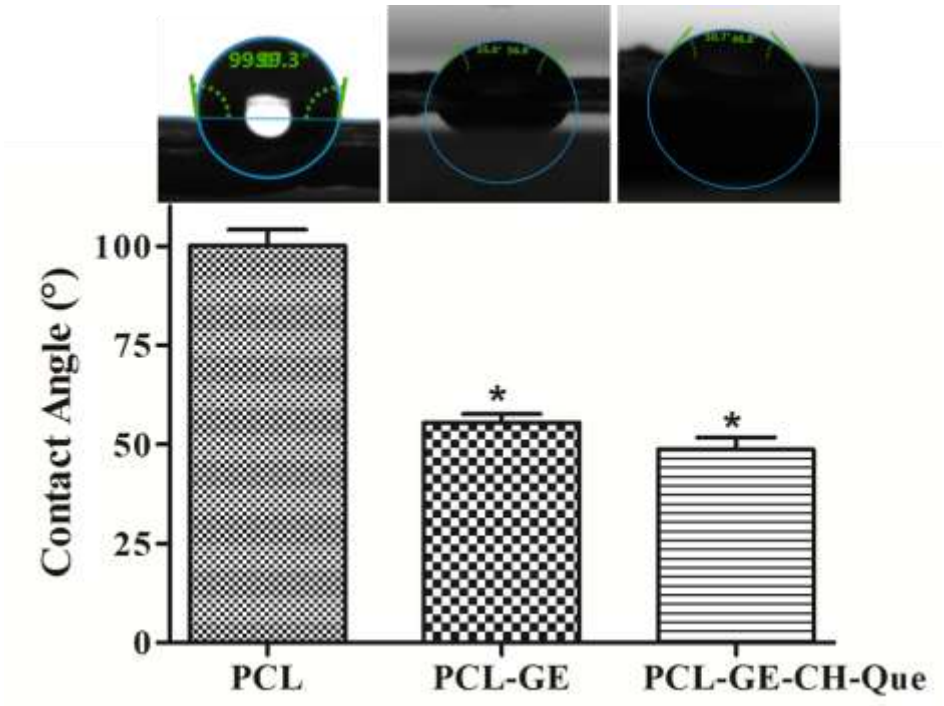

Figure 5.21: Water droplet profile and quantitative value of contact angle for PCL (100.1±3.958°), PCL-GE (55.5±2.095°), and PCL-GE-CH-Que nanofibers (48.76±2.950°). The data are expressed as mean and vertical bar represents SD (n=3). *p<0.05 vs PCL nanofibers.

5.3.4. Entrapment efficiency and *in-vitro* cumulative drug release study

Entrapment efficiency of fabricated nanofiber membranes is shown in Table 5.9. High entrapment efficiency of nanofibers might be due to better miscibility of drugs with polymers which results in good interaction of drugs with the polymer matrix and enhanced dispersion of drugs in nanofibers. Further, the non-volatile nature of drugs and mixing of optimum concentration of drugs resulted into partial loss of drugs as aggregate on the nanofibers surface during in-situ solidification of the drugs-polymers mixture. Therefore, fabricated nanofibers entrapped most of the drugs with a fractional amount appeared on the surface, which also confirmed the assumption of XRD outcome.

The release profile of ciprofloxacin hydrochloride and quercetin from PCL-GE-CH-Que nanofibers in phosphate buffer (pH 7.4) is displayed in Figure 5.22. It has been observed that release of entrapped drugs from nanofibers was biphasic in nature, with initial burst release followed by sustained release. The probable reason for the initial burst release was quick solubilization of amorphous surface-aggregate, and also due to leaching of drugs which was entrapped near the surface and was in direct contact of dissolution media. The reason for the extended release could be longer diffusion path from thick nanofibers, slow biodegradation of gelatin due to entanglement with PCL chains, and the crystallinity of PCL [Xue et al. 2014]. Since the underlying objective was to minimize the microbial infection and thus reduced generation of ROS during the initial healing phase, therefore, the burst release of drugs was deemed necessary, and this had been observed in PCL-GE-CH-Que nanofibers release profile. Further, the addition of gelatin increased the degradation of nanofibers which resulted into 99.18% (ciprofloxacin hydrochloride) and 88.09% (quercetin) release in 4 days as shown in Table 5.10.

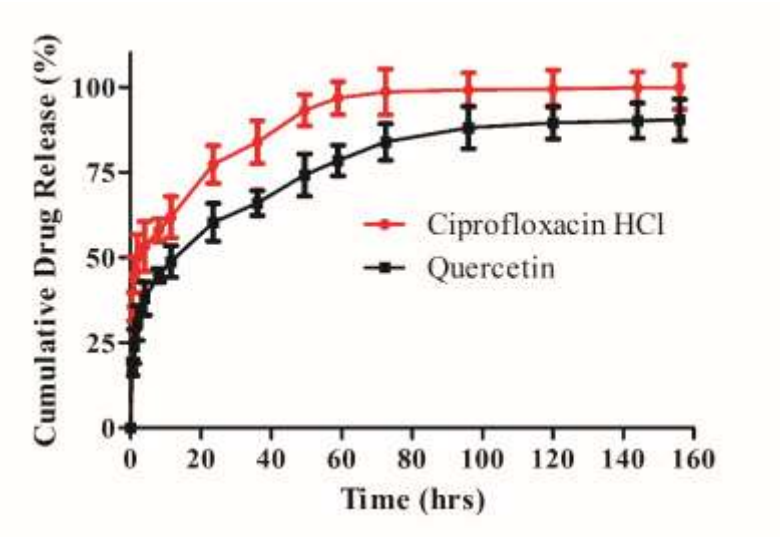

Figure 5.22: *In-vitro* release profiles of quercetin and ciprofloxacin hydrochloride from PCL-GE based nanofibers in phosphate buffer (pH 7.4). The data are expressed as mean and vertical bar represents SD (n=3).

Table 5.10: *In-vitro* drug release data of PCL-GE based nanofiber membrane in phosphate buffer (pH 7.4)

Time (h)	Cumulative Percentage Drug Release	
	Ciprofloxacin Hydrochloride	Quercetin
0	0.00	0.00
0.5	35.60±4.23	17.79±2.41
1	44.93±5.30	23.96±4.99
2	49.98±6.82	30.79±5.03
4	53.21±7.30	37.91±4.85
8	57.98±3.39	44.78±2.01
11.5	61.82±6.02	48.80±4.67
23.5	77.30±5.56	60.31±5.52
36	83.79±6.24	65.97±3.68
49.5	93.18±4.60	74.16±6.17
59	96.71±4.85	78.41±4.51
72.5	98.56±6.72	83.88±5.37
96	99.18±4.98	88.09±6.16
120	99.45±5.46	89.54±4.80
144	99.82±4.61	90.09±5.19
156	99.90±6.45	90.39±6.04

The values are expressed as mean±SD (n=3).

5.3.5. *In-vitro* antibacterial activity

Inhibition of bacterial growth zone was used to determine anti-bacterial property of nanofibers. The growth of *S. aureus* can be observed directly from the petri-dish to evaluate the antibacterial property (Figure 5.23 (a) & (b)). Figure 5.23 (c) represents the diameter of inhibition zone with respect to different incubation time and the values of same are shown in Table 5.11. It can be observed that placebo nanofibers (F_1) did not show any antibacterial activity throughout the study period. In contrast, PCL-GE-CH (F_2) and PCL-GE-CH-Que (F_3) nanofibers exhibited wide inhibition zone initially which might be due to rapid release of antimicrobial. Although, PCL-GE-CH-Que had a little broad inhibition zone in comparison to PCL-GE-CH, but except on day 3 no significant difference had been observed between their values. Hence, it could be established that electrospun nanofibers was sufficiently active to check the bacterial growth during the experimental period and electrospinning did not change the antimicrobial property of ciprofloxacin hydrochloride while encapsulating in the nanofibers.

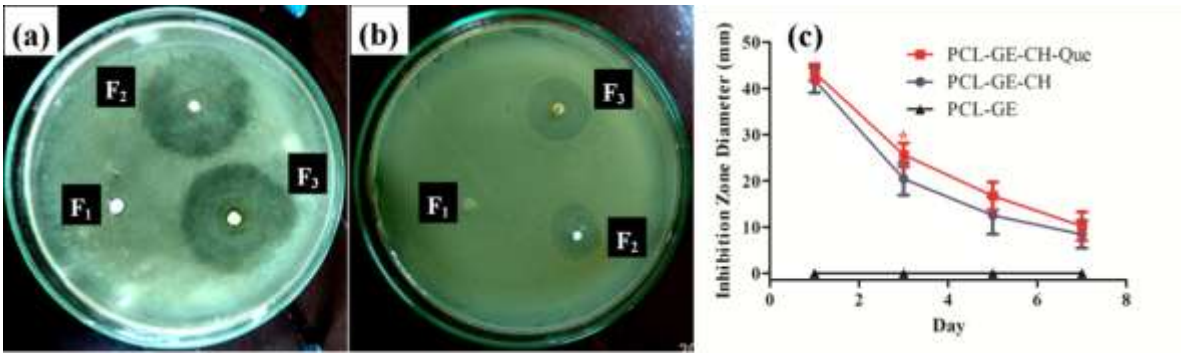

Figure 5.23: Antimicrobial activity of nanofiber membranes against *S. aureus*: (a)inhibition zone on day 1, (b) inhibition zone on day 3, (c) graphical illustration showing the relationship between diameters of inhibition zone (mm) vs incubation time (days). F_1, F_2, and F_3 represent the PCL-GE, PCL-GE-CH, and PCL-GE-CH-Que nanofibers, respectively. The data are expressed as mean and vertical bar represents SD (n=3). *$p<0.05$ vs PCL-GE-CH nanofibers.

Table 5.11: Diameter of *S. aureus* inhibition zone on agar plate after incubation with different PCL-GE based nanofiber membranes.

Time (days)	PCL-GE Nanofibers	PCL-GE-CH Nanofibers	PCL-GE-CH-Que Nanofibers
1	0	41.78±2.76	43.42±1.8
3	0	20.4±3.53	25.63±2.57
5	0	12.52±4.05	16.71±3
7	0	8.4±2.950469	10.2±3.1

The values are expressed as mean±SD (n=3).

5.3.6. Free-radical scavenging efficiency of nanofibers

The Free-radical scavenging efficacies of the nanofibers were established by DPPH reduction method and shown in Figure 5.24. The assay is based on the principle that DPPH is stable free-radical and it gives purple color solution in methanol. After accepting an electron or hydrogen from an antioxidant, it reduces to $DPPH_2$ and solution color changes to yellow. This change in color is measured at λ_{517nm} and utilized for estimation of relative antioxidant efficacies of different nanofibers [Selvaraj and Fathima 2017]. It was found that PCL-GE nanofibers scavenged the 8.69% DPPH, which might be due to gelatin-derived radical-scavenging peptide sequence (His-Gly-Pro-Leu-Gly-Pro-Leu) [Mendis et al. 2005]. Further, quercetin loaded nanofibers quenched the 55.14% DPPH, which proved the antioxidant activity of phenolic groups present in the quercetin.

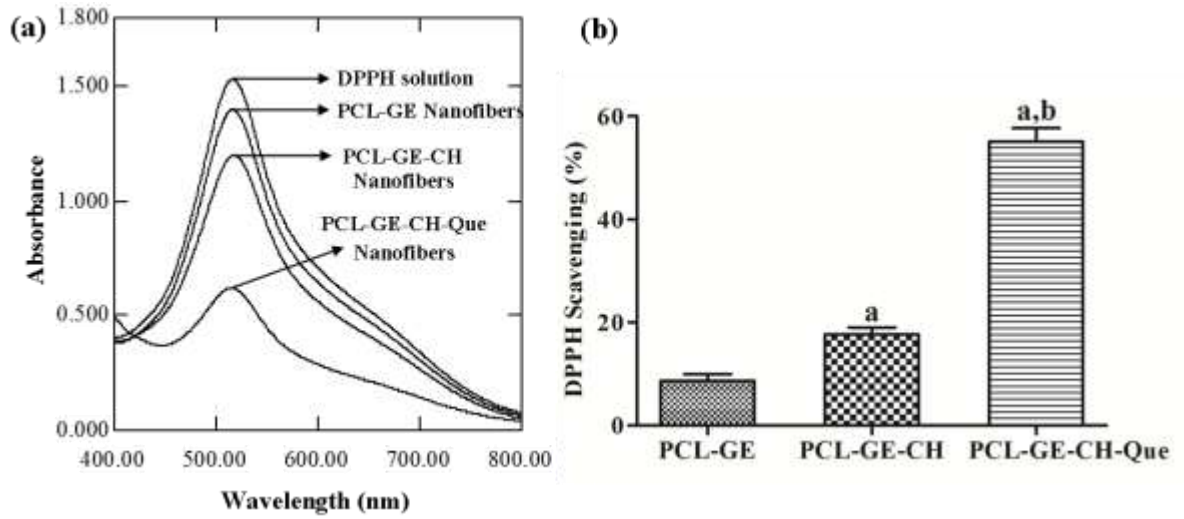

Figure 5.24: Free radical scavenging efficacies of the PCL-GE, PCL-GE-CH, and PCL-GE-CH-Que nanofibers after 0.5h incubation with DPPH solution: (i) UV-Vis spectra; (ii)histogram representing DPPH attenuation efficiencies of different nanofibers. The data are expressed as mean and vertical bar represents SD (n=3). $^{a}p<0.05$vs PCL-GE nanofibers, $^{b}p < 0.05$ vs PCL-GE-CH nanofibers.

5.3.7. Biocompatibility study

5.3.7.1. Hemocompatibility assessment of nanofiber membrane

Percentage hemolysis represents the degree of erythrocytes lysed when they are exposed to the nanofibers in the solution. A higher value of hemolysis indicates the poor hemocompatibility of the nanofibers intended for application. The influence of different nanofiber membrane on the integrity of erythrocytes is shown in Figure 5.25. The degree of erythrocytes broken-down in the presence of PCL-GE-CH-Que nanofibers was 1.072%, which was significantly ($p < 0.05$) much lower in comparison to other nanofibers. Although other nanofibers caused higher hemolysis in comparison to PCL-GE-CH-Que, all results were under the acceptable range of 5% [Haghjooy Javanmard et al. 2016]. The plausible reason for the low value of hemolysis caused by PCL-GE-CH-Que nanofibers was protective action of quercetin, a flavonoid, which diminished the peroxidation of

unsaturated fatty acid and oxidative damage of glutathione and thiol group (-SH) in the erythrocytes membrane.

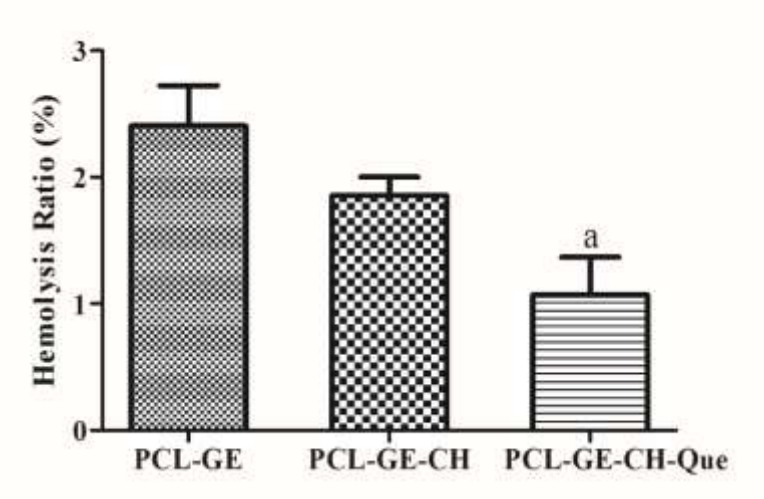

Figure 5.25: *In-vitro* hemocompatibility of PCL-GE, PCL-GE-CH and PCL-GE-CH-Que nanofibers. The data are expressed as mean and vertical bar represents SD (n=3). $^{a}p < 0.05$ vs PCL-GE nanofibers.

5.3.7.2. Cytocompatibility assessment of nanofiber membrane

The viability of 3T6-Swiss albino fibroblast on the nanofibers was evaluated by MTT assay, and the results are displayed in Figure 5.26. It was observed that the cells proliferated well on all the nanofiber membranes indicating the cytocompatible and nontoxic nature. All nanofibers showed more than 100% cell viability even after 72h incubation, which might be due to cell recognition site (Arg-Gly-Asp amino acid sequence) provided by gelatin protein and thus high cell adhesion and proliferation on gelatin nanofibers. The significantly ($p < 0.05$) higher cell viability on PCL-GE-CH-Que nanofiber surface was attributed to additional protective nature offered by quercetin, a flavonoid, which was found to increase the fibroblast proliferation and collagenesis as reported by Selvaraj and Fathima, 2017.

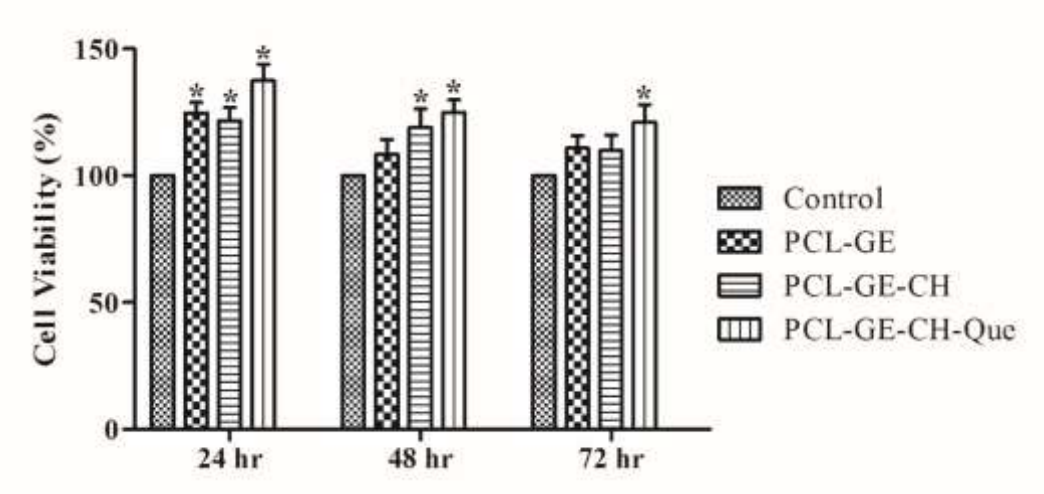

Figure 5.26: Viability of Swiss albino 3T6 fibroblast cells on nanofibrous scaffolds after 24h, 48h and 72h incubation times. The data are expressed as mean and vertical bar represents SD (n=3). *p<0.05 vs control. A cell suspension cultured into a well without any scaffold was considered as control.

5.3.8. *In-vivo* wound healing study

Throughout the sixteen days of the treatment period, no animals showed any post-operative adverse reaction such as bleeding of granulation tissue, fluid retention, infection, sepsis, etc. All the animals stayed alive till the end of the experiment and by the end of 3rd week all the groups exhibited complete healing. Figure 5.27 (a) showed the representative images of rats from all the four groups (gauze, PCL-GE, PCL-GE-CH, and PCL-GE-CH-Que treated) on 8th and 16th day after grafting and Figure 5.27 (b) showed wound area closed during the experimental period. Among the four groups, all the treated groups showed excellent adherence and complete degradation and assimilation of nanofibers in the granulation tissue, which was due to hydrophilicity provided by the gelatin and they also exhibited significant ($p<0.05$) wound healing in comparison to gauze treated group. Native ECM mimicking structure provided by nanofibers and cell-recognition site (Arg-Gly-Asp amino acid sequence) on gelatin might have increased the cell attachment and its spreading. Since the day 12, sealing effect had been observed in case of PCL-GE-CH-Que treated group and

no significant difference was observed in wound area closure between day 12 and day 16. On day 16, PCL-GE-CH-Que treated group provided nearly 100% wound closure, whereas wound closed by PCL-GE-CH, PCL-GE and gauze treated group was 89.08%, 78.85% and 71.32%, respectively.

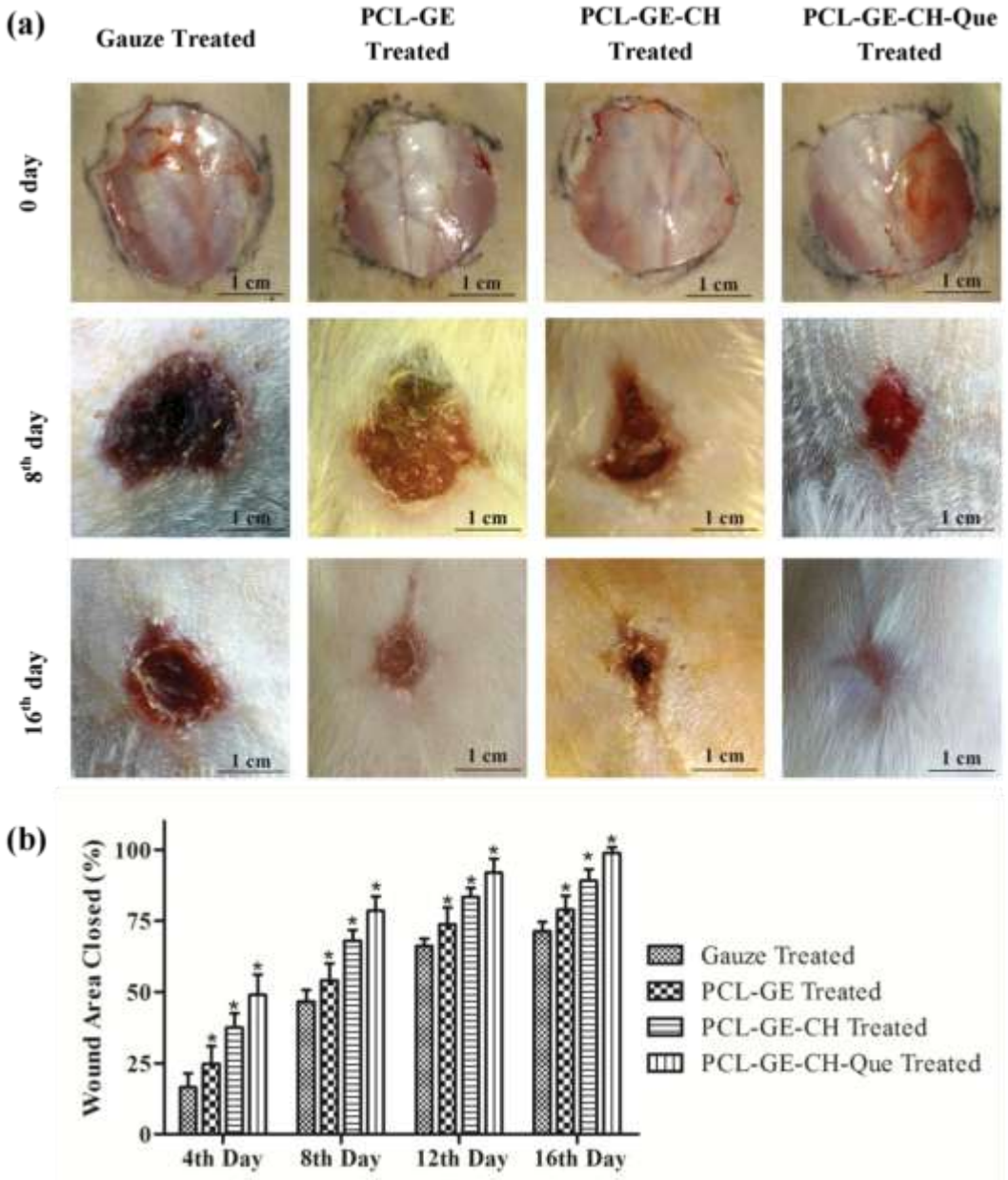

Figure 5.27: Effect of nanofibers for the healing of full thickness wound: (a) representative images of wound healing on day 8 and 16, (b) percentage of wound area closed following treatment with gauze, PCL-GE, PCL-GE-CH and PCL-GE-CH-Que nanofibers on day 4, 8, 12 and 16. The data are expressed as mean and vertical bar represents SD (n=3). *$p < 0.05$ vs gauze treated.

5.3.8.1. Histological examination of granulation tissues

The histological changes of gauze and nanofibers treated groups were evaluated by haemotoxyline & eosin staining of granulation tissue on 8^{th} and 16^{th} days and results are displayed in Figure 5.28. On day 8, the surface layer of granulation tissue of gauze treated group showed high ulceration and the underlying layer was severely infiltrated with inflammatory cells. The wound in PCL-GE and PCL-GE-CH treated group displayed granulation tissue with moderate ulceration and infiltration with inflammatory response and with fewer fibroblasts. In contrast, PCL-GE-CH-Que nanofibers treated group demonstrated moderate epithelialization. The amount of inflammatory response at this stage in the PCL-GE-CH-Que nanofibers treated group was quite low in comparison to other groups, confirming the anti-oxidant activity of nanofibers. Moderate amount of fibroblast in PCL-GE-CH-Que nanofibers treated granulation tissue established its accelerated healing property.

On day 16, PCL-GE-CH-Que nanofibers treated group exhibited complete re-epithelialization. The epidermal layer was thick and infiltrated with keratinocyte while dermal layer had good collagen deposition and spars inflammatory cells, demonstrating complete wound healing. The wound treated with PCL-GE-CH nanofibers also exhibited good re-epithelialization, fever infiltration with inflammatory response and comparatively more white space indicating moderate collagen deposition in comparison to PCL-GE-CH-Que nanofibers treated group. Gauze treated wound showed moderate re-epithelialization with inflammatory infiltration, necrotic fibrinoid debris, poor collagen deposition, and capillary hyperproliferation, signifying that inflammation was still present in this group.

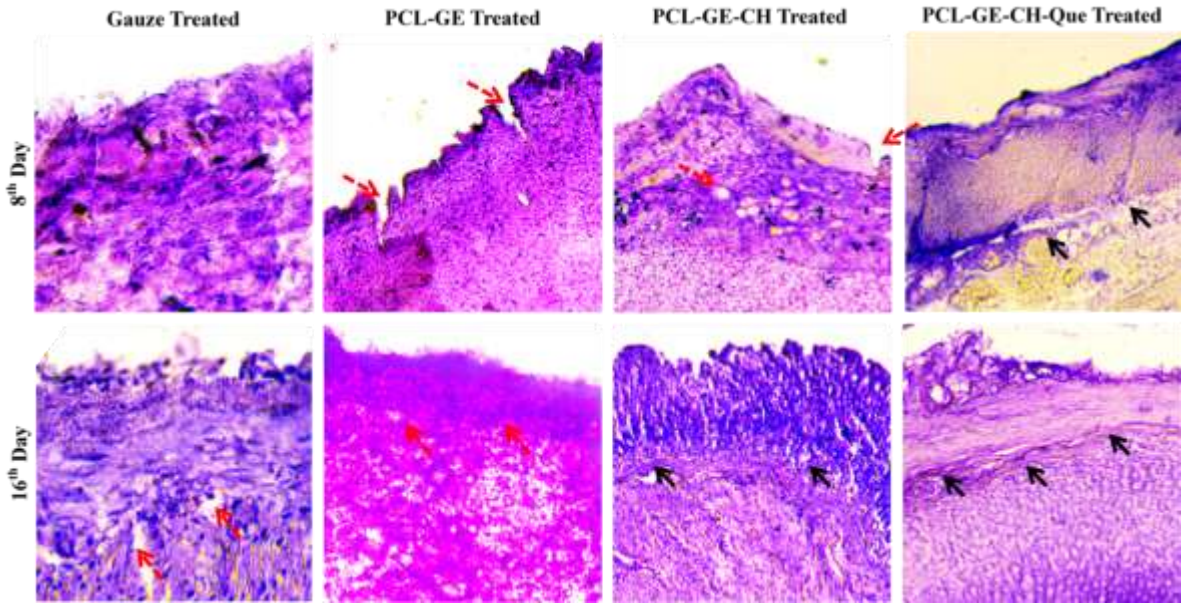

Figure 5.28: Histological changes in granulation tissue of gauze, PCL-GE, PCL-GE-CH and PCL-GE-CH-Que nanofibers treated groups on day 8 and 16. Optical magnification was 10X. The black color arrow indicates growth of dermis and epidermis layer while red color arrow indicates lack of collagen synthesis in the dermis region.

5.3.8.2. Antioxidant enzyme activity in granulation tissues

Open full thickness wound is very prone to microbial infection which results into excessive production of ROS and thus oxidative damage of fibroblast and collagen metabolism. During inflammatory phase of wound healing (1-4 days), even quercetin, an exogenous antioxidant, was not able to enhance the activity of SOD and catalase significantly (Figure 5.29). Although, PCL-GE-CH-Que treated group shown a significant improvement ($p < 0.05$) in SOD and catalase level in contrast to other treated group, still a significant difference ($p < 0.05$) was found when compared with control group. PCL-GE-CH treated group maintained a significant ($p < 0.05$) improvement in enzymes level throughout the experiment period when compared to gauze and PCL-GE treated group, which might be due to attenuation of bacterial invasion and therefore low ROS generation. On day 16, only PCL-GE-CH-Que treated group achieved SOD level up to control groups ($p > 0.05$, non-

significant difference), however, a significant difference ($p < 0.05$) was still found in catalase level. Therefore, antimicrobial and antioxidant property of nanofibers would be helpful for attenuating ROS and attaining the endogenous anti-oxidant level up to homeostatic state.

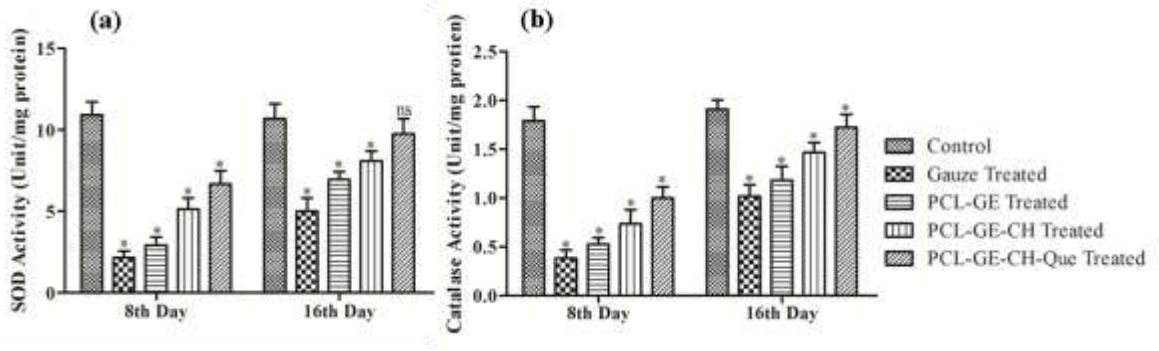

Figure 5.29: Effect of treatment with different nanofibers on endogenous enzymes viz. (a)SOD and (b) catalase in granulation tissues on day 8 and 16. The data are expressed as mean and vertical bar represents SD (n=3). *$p < 0.05$ vs control group and $^{ns}p > 0.05$ vs control group.

5.3.8.3. Hydroxyproline content in granulation tissues

On day 8, although all nanofibers treated groups began to achieve statistically significant ($p<0.05$) increase in hydroxyproline contents as compared to gauze treated, but no one could reach to an insignificant difference level in comparison to control group (Figure 5.30). On day 16, hydroxyproline content peaked in PCL-GE-CH-Que nanofibers treated group, which was 2.531±0.239 µg/mg of granulation tissue and no significant difference was found when compared with the control group. Although, hydroxyproline content in PCL-GE-CH nanofibers treated group was quite high in comparison with gauze treated and PCL-GE nanofibers treated group, but still a significant difference exist between PCL-GE-CH nanofibers treated group and control group.

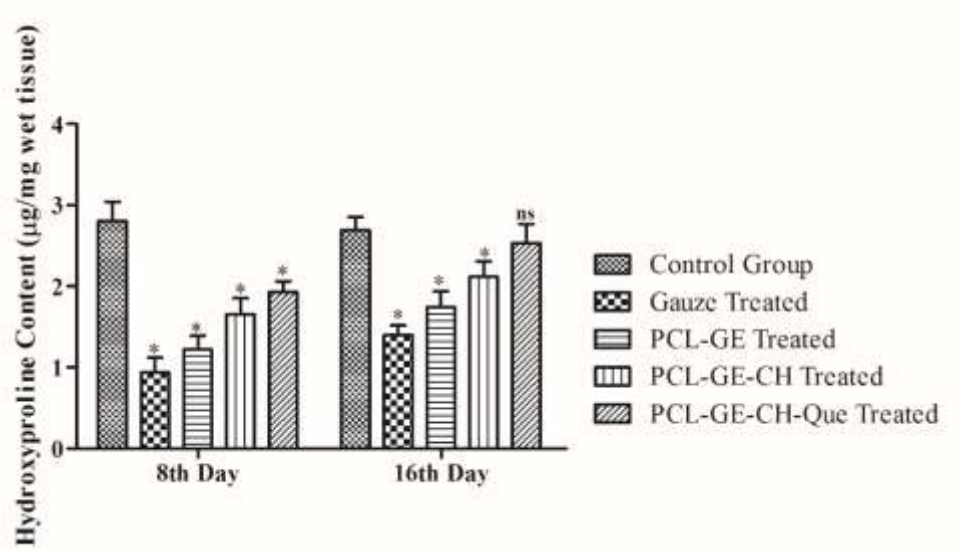

Figure 5.30: Effect of different nanofibers on hydroxyproline content in granulation tissue of rats on day 8 and 16 post-wounding. The data are expressed as mean and vertical bar represents SD (n=3). *$p<0.05$ vs control group and $^{ns}p>0.05$ vs control group.

Although blending of gelatin with PCL resulted in significantly fast *in-vitro* degradation rate, hydrophilicity and hence attachment at the wound site with comparatively higher cost (PCL 440744-500G: Rs 21,974.57 + Gelatin MB169-500G: Rs 4200) and optimum mechanical strength than PCL based scaffold, however, PCL-GE solution separated into two phases during long-duration electrospinning and requires continuous mixing. Further, due to PCL content, the resulting nanofibers membrane did not biodegrade and assimilates completely during the course of healing. As per Schneider et al. [Schneider et al. 2007] during wound healing a temporary physiological acidosis was observed due to generation of lactic acid and other factors. A mild acidosis might be beneficial for fibroblast migration, DNA synthesis and hence wound healing. Therefore, taking into consideration of above mentioned problems of PCL-GE based nanofiber membrane and advantages of mild acidosis, we have proposed to blend gelatin with PLGA polymers, which upon hydrolytic degradation releases biocompatible monomers, namely lactic acid and glycolic acid. This

lactic acid causes mild acidosis in microenvironment and help in wound healing. Further, PLGA also offers complete mixing with gelatin and high predictability of release kinetic, and had been used since long time in suture and other marketed formulations [Ulery et al. 2011].

5.4. Fabrication and Characterization of PLGA-GE Based Nanofibers Loaded with Ciprofloxacin Hydrochloride and Quercetin

PLGA-GE based nanofibers of different composition were fabricated successfully using hexafluoro-2-propanol solvent. HFIP is most frequently used solvent for biopolymers electrospinning since it breaks the hydrophobic interaction between natural polymers, forms strong hydrogen-bond and solubilize them [Nguyen et al. 2012, Zhang et al. 2010]. In addition, owing to relatively low boiling point (60°C), HFIP volatilize very rapidly while electrospinning and also from the resulting nanofibers [Bide et al. 2010]. Various properties of fabricated nanofibers such as morphology, average diameter (nm), membrane porosity (%) and entrapment efficiency (%) are shown in Table 5.12.

Table 5.12: Morphology, porosity and entrapment efficiency of different PLGA-GE based nanofibers.

Sample	Fiber Morphology	Average Diameter (nm)*	Membrane Porosity (%)	Entrapment Efficiency (%)
Gelatin (GE)	Smooth & thin nanofibers	241.970±65.294	69.62%	-
PLGA-GE	Smooth, thick nanofibers with fibrils	504.724±182.703	81.21%	-
PLGA-GE-CH	Smooth nanofiber with frequent breakage	577.393±231.221	75.90%	CH: 91.56
PLGA-GE-CH-Que	Smooth nanofibers with fewer fibrils and uniform size distribution	642.489±301.039	72.53%	CH: 92.04 Que: 94.32

*The data are expressed as mean±SD, n=100

5.4.1. Morphology of electrospun nanofibers

The morphology and diameter distribution of gelatin (a,b), PLGA-GE (c,d), PLGA-GE-CH (e,f), and PLGA-GE-CH-Que nanofiber membrane (g,h) are shown in Figure 5.31. The SEM images exhibit randomly oriented, smooth nanofibers with broader size distribution. All nanofibers showed fibrous structure with interlocked pores. This architecture ideally mimics the physical structure of extracellular matrix and has proven to be appropriate for cell migration, adhesion, proliferation, and differentiation. The mean diameter of gelatin, PLGA-GE, PLGA-GE-CH, and PLGA-GE-CH-Que nanofibers was 241.97±65.29 nm, 504.72±182.70 nm, 577.39±231.22 nm, and 642.49±301.04 nm, respectively. Probable reason for significantly increased diameter of PLGA-GE nanofibers in comparison to gelatin nanofibers was reduction of charge-density generated by amino acids of gelatin, and hence low stretching and bending, as also reported by Meng et al., [Meng et al. 2010]. Further loading of drugs in PLGA-GE matrix caused the nanofibers production with increased average diameter, smooth surface and more uniform size distribution.

Porosity becomes a vital parameter while selecting a nanofibers for tissue regeneration. The ideal porosity for tissue-engineered membrane intended for skin regeneration should be in the range of 60-90% [Chong et al. 2007]. The porosity in this range should be beneficial for the adherence, in-growth, and proliferation of fibroblast on the nanofibers. Further, this will assist in gases, nutrient, and exudates exchange across the membrane. As indicated in Table5.12, the porosity of fabricated nanofibers is within this range, which ensures their application for skin regeneration.

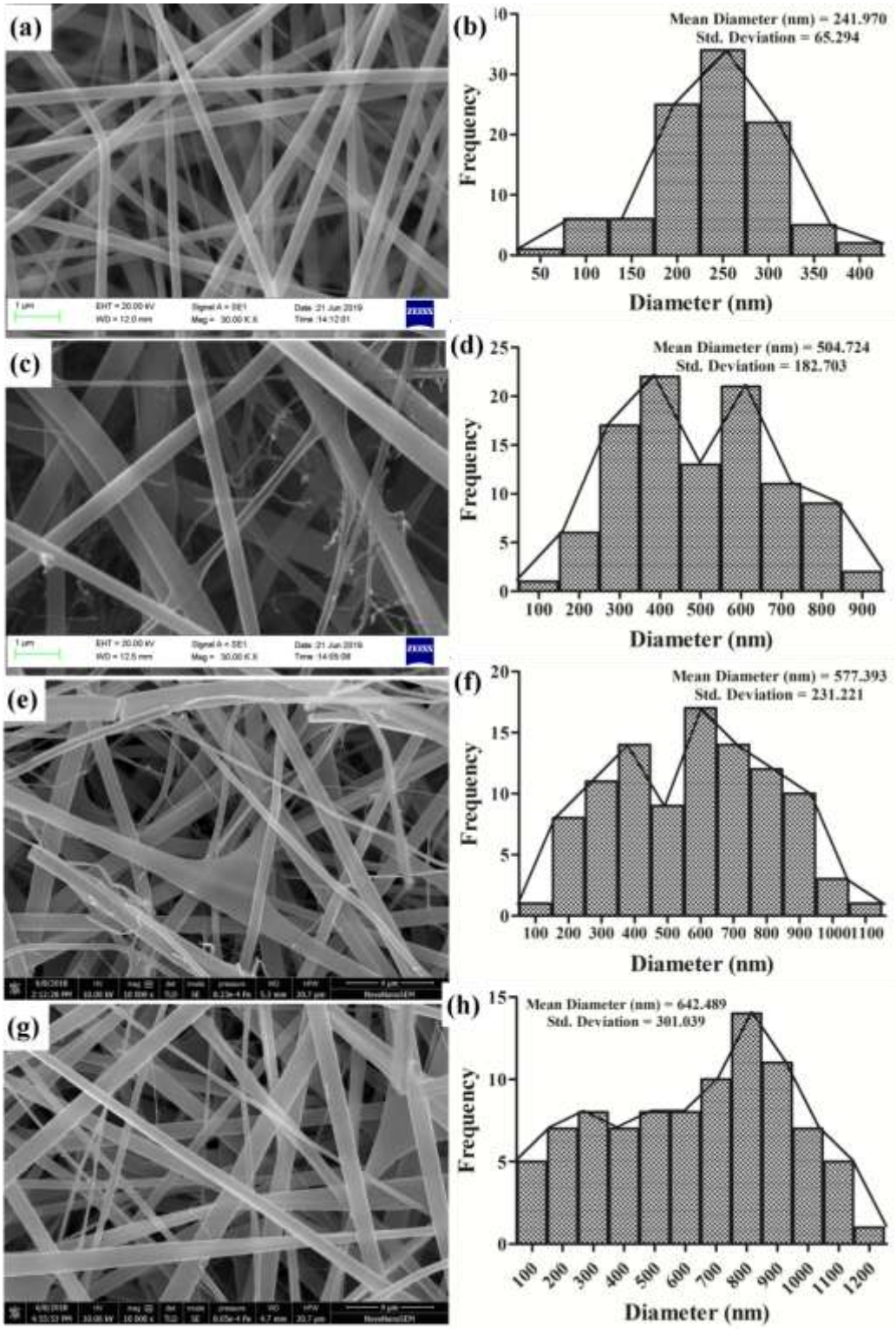

Figure 5.31: The HSEM micrograph of nanofibers and histogram of fiber diameter with respect to its distribution frequency: (a,b) gelatin nanofibers, (c,d) PLGA-GE nanofibers, (e,f) PLGA-GE-CH nanofibers, and (g,h) PLGA-GE-CH-Que nanofibers. The data are expressed as mean±SD, n=100.

5.4.2. Solid-state characterizations

FT-IR spectroscopy was performed to investigate any possible drug(s) and polymer(s) interactions, effect of electrospinning on drug(s) stability and functional groups of drugs entrapped in nanofibers [Gaonkar et al. 2017, Khan et al. 2017]. FTIR spectra CH, Que, PLGA-GE nanofibers, and PLGA-GE-CH-Que nanofibers are presented in Figure 5.32. Ciprofloxacin Hydrochloride showed its characteristic peak at 804.34 cm^{-1} for C-F stretching vibration, 1624.11 cm^{-1} for ketone C=O stretching vibration, 1708.99 cm^{-1} for carboxylic acid C=O stretching vibration, and a broad shoulder between 3350-3550 cm^{-1} for N-H and O-H stretching vibration. Similarly, the crystalline nature of quercetin revealed by peaks at 1383 cm^{-1} for O-H bending vibration of phenol functional group, 1664.62 cm^{-1} for aryl ketone C=O stretching vibration and a broad peak around 3400 cm^{-1} correspond to stretching vibration of five O-H phenolic groups. Due very low amount of drugs in the electrospun nanofibers, PLGA-GE-CH-Que spectra showed diminished peaks of CH and Que. Further, some peaks of drugs were masked by polymers' peaks. Since drugs loaded nanofibers was releasing the drugs in dissolution media, inhibiting microbial growth on agar plate, and attenuating the DPPH free radicals in methanol solution, therefore, drugs-polymers interaction and change of drugs chemical nature could be ruled-out. It can therefore be concluded that drugs and polymers are chemically compatible.

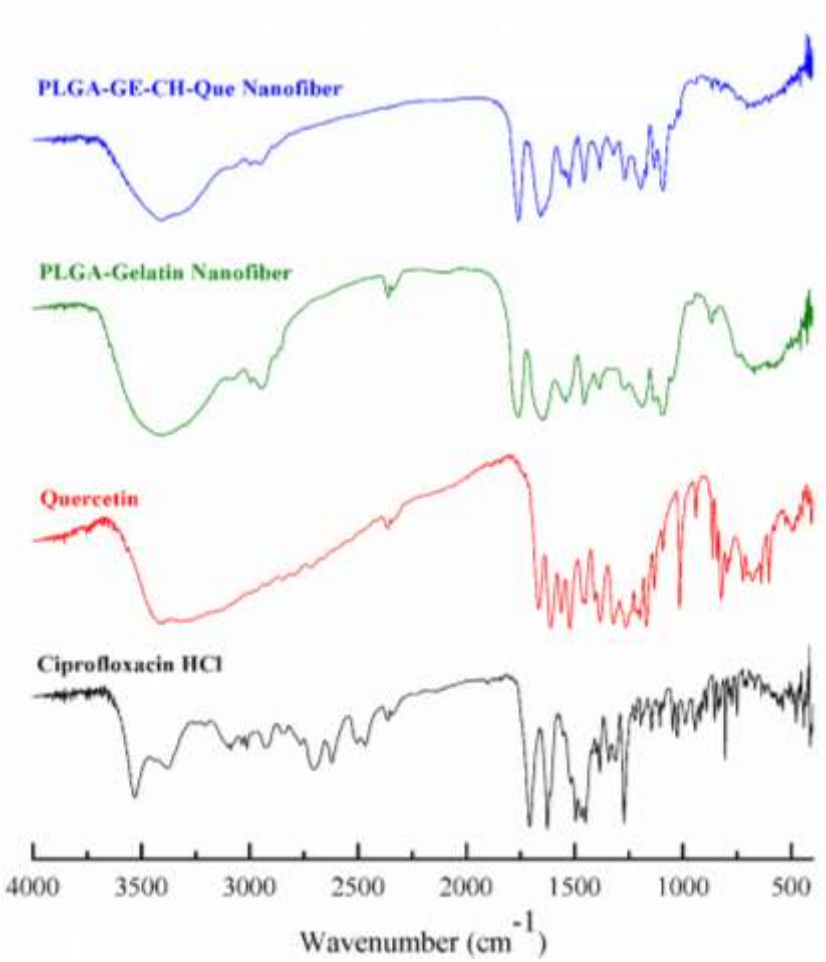

Figure 5.32: Chemical characterization of ciprofloxacin hydrochloride, quercetin, PLGA-GE nanofibers and drug loaded PLGA-GE based nanofibers via FT-IR.

To demonstrate the physical state of entrapped drugs, XRD patterns of CH, Que, PLGA, gelatin and drugs loaded nanofibers were examined during the study and are displayed in Figure 5.33. Ciprofloxacin hydrochloride spectra showed few sharp diffraction peaks at 8.2°, 9.04°, 19.3°, 24.72°, and 26.48° in addition with other minute peaks, which refers to the crystalline nature of the drug, which was consistent with the finidng of previous studies [Kataria et al. 2014]. Similarly, few sharp peaks at 10.74°, 12.42°, 27.34° signified the crystalline nature of quercetin, which was also observed by Qi et al., [Qi et al. 2015]. Furthermore, XRD spectra of gelatin and PLGA exhibited only a broad shoulder and

devoid of any sharp peak, which signifies their amorphous nature. However, the XRD spectra of PLGA-GE-CH-Que nanofibers did not exhibit characteristic peaks of either drugs, which signified that a fraction of the drugs were entrapped in the nanofibers and the remainder of the quantity was aggregated on the surface of the nanofibers in amorphous form, as rapid *in-situ* solidification did not provide adequate time for recrystallization of the drug molecules on nanofibers surface. The initial burst release of drugs during *in-vitro* release study of the nanofibers further verified this observation.

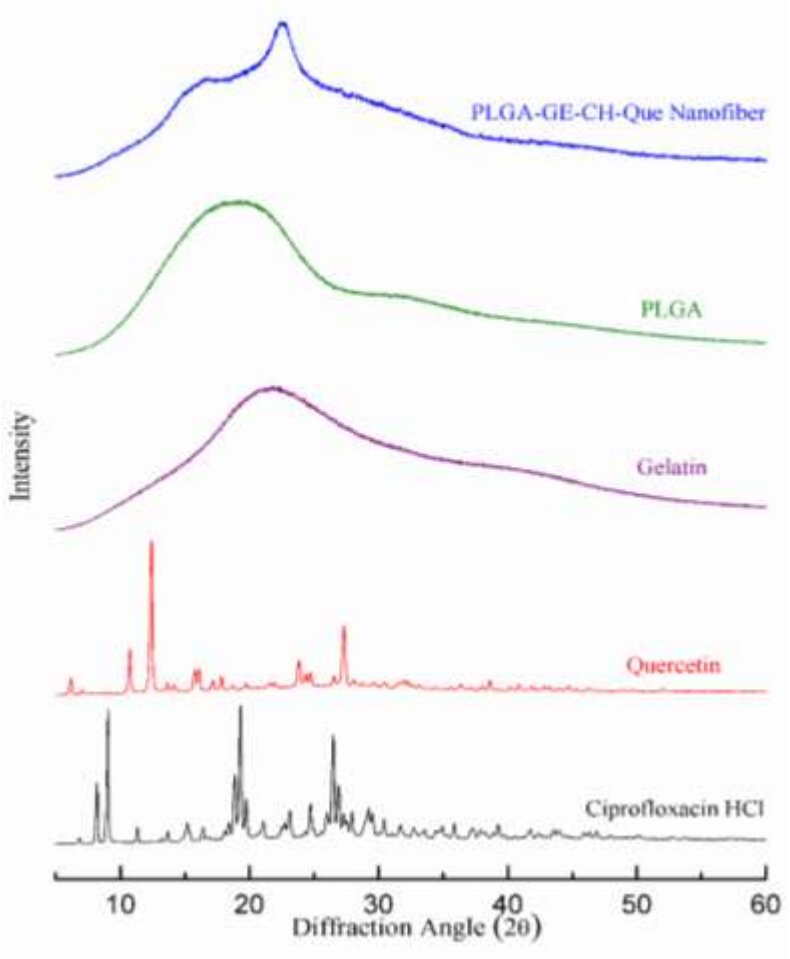

Figure 5.33: Overlay XRD spectra of ciprofloxacin hydrochloride, quercetin, gelatin, PLGA and drug loaded PLGA-GE based nanofibers.

5.4.3. Entrapment efficiency and *in-vitro* cumulative drug release study

As only in-situ solidification of the solution occurs during electrospinning, the entrapment efficiency of nanofibers should, therefore, be nearly 100%, taking into account the complete miscibility of the drug and polymer, non-volatile nature of the drug and the optimal concentration of the drug. The encapsulation efficiency decreases at higher concentrations of the drugs, mostly because of excess drug losses as an aggregate on the surface of nanofibers which escape encapsulation in nanofibers. The fabricated PLGA-GE-CH-Que nanofiber displayed high entrapment efficiency as shown in Table 5.12.

The drug release profiles of ciprofloxacin hydrochloride and quercetin from PLGA-GE-CH-Que nanofiber membrane was evaluated in phosphate buffer (pH 7.4) and shown in Figure 5.34. The release of encapsulated drugs occurred in a biphasic manner, with an initial burst release followed by sustained drugs release. The possible reason for the initial burst release was quick solubilization of amorphous surface-aggregate and also due to leaching of drugs which was entrapped near the surface and being in direct contact of dissolution media. Ciprofloxacin hydrochloride is more soluble in phosphate buffer than quercetin; therefore, it showed more burst release (63.56%) than quercetin (51.43%) as shown in Table 5.13. The probable reason for the sustained release could be longer diffusion path from the thick nanofibers and also slow biodegradation of PLGA-GE chain. Since the underlying objective of the PLGA-GE-CH-Que nanofibers release profile was to minimize the microbial infection and thus reduced generation of ROS at the wound site, hence initial burst release was considered necessary. Further, the addition of gelatin increased the degradation of nanofibers which resulted into 97.42% (ciprofloxacin hydrochloride) and 80.21% (quercetin) release in 49 h (around 2 days).

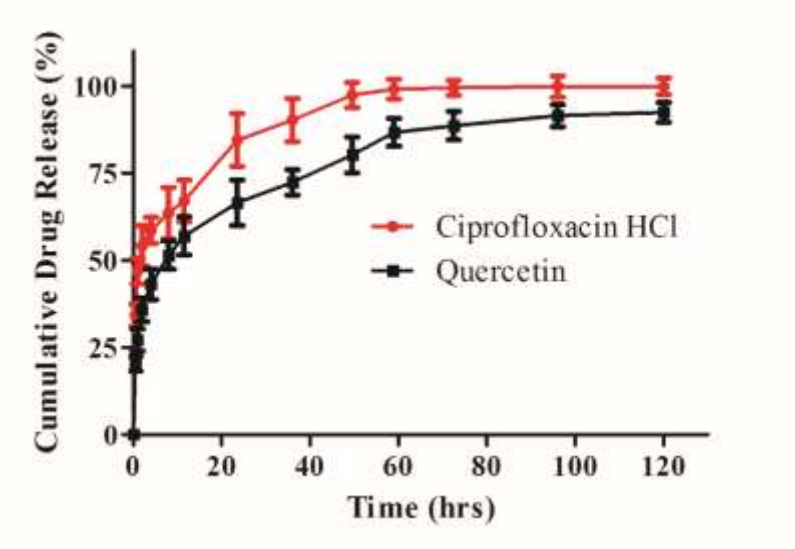

Figure 5.34: *In-vitro* release profiles of ciprofloxacin hydrochloride and quercetin from PLGA-GE based nanofibers in phosphate buffer (pH 7.4). The data are expressed as mean and vertical bar represents SD (n=3).

Table 5.13: *In-vitro* drug release data of PLGA-GE based nanofiber membrane in phosphate buffer (pH 7.4)

Time (h)	Cumulative Percentage Drug Release	
	Ciprofloxacin Hydrochloride	Quercetin
0	0.00	0.00
0.5	34.20±3.23	20.33±2.11
1	46.93±3.70	27.12±3.19
2	54.14±5.82	35.88±3.43
4	58.53±3.80	43.10±4.35
8	63.56±7.39	51.44±4.02
12	67.02±6.02	57.01±5.47
24	84.50±7.56	66.50±6.52
36	90.21±6.24	72.38±3.68
49	97.43±3.60	80.21±5.17
59	99.12±2.85	86.70±4.01
72	99.47±2.12	88.63±4.07
96	99.85±3.08	91.50±3.16
120	99.90±2.34	92.45±2.80

The values are expressed as mean±SD (n=3).

5.4.4. *In-vitro* antibacterial activity

Antibacterial efficacies of fabricated nanofibers were evaluated by film diffusion method against *S. aureus*. The inhibition of *S. aureus*' growth on agar plate can be visualized directly from Figure 5.35 (a) and (b), and relation between inhibition diameters with regards to incubation time is displayed in Figure 5.35 (c). It can be noted that throughout the research period, PLGA-GE nanofibers (F1) showed no antibacterial activity. In contrast, PLGA-GE-CH (F2) and PLGA-GE-CH-Que (F3) nanofibers initially demonstrated wide inhibition zone that could be attributed to burst antimicrobial release. Later, these nanofibers displayed decreasing order of inhibition zone with time, which could be due to slow and sustained release of antimicrobial agents. Therefore, it could be stated that electrospun nanofibers was sufficiently active during the experimental period to check bacterial growth and that electrospinning process did not change the antibacterial property of ciprofloxacin hydrochloride while encapsulating in the nanofibers.

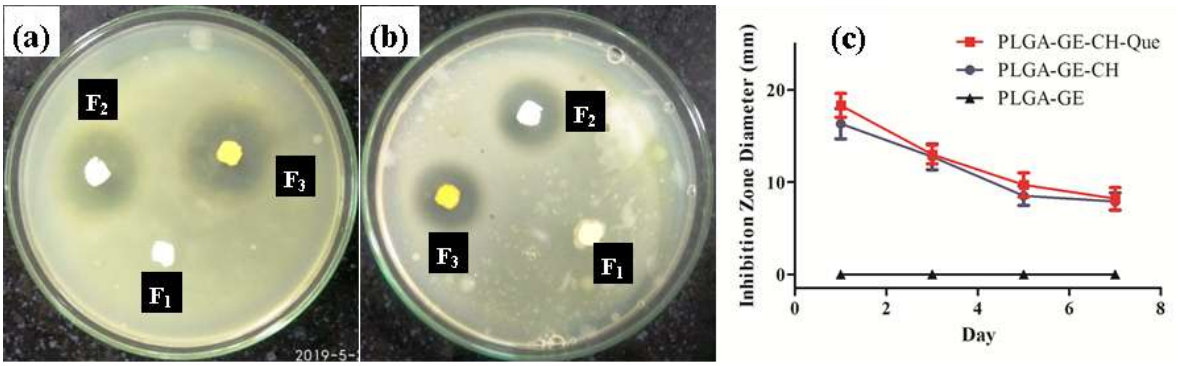

Figure 5.35: Antimicrobial activity of nanofiber membranes against *S. aureus*: (a)inhibition zone on day 1, (b) inhibition zone on day 3, (c) graphical illustration showing the relationship between diameters of inhibition zone (mm) vs incubation time (days). F_1, F_2, and F_3 represent the PLGA-GE, PLGA-GE-CH, and PLGA-GE-CH-Que nanofibers, respectively. The data are expressed as mean and vertical bar represents SD (n=3).

Table 5.14: Diameter of *S. aureus* inhibition zone on agar plate after incubation with different PLGA-GE based nanofiber membranes.

Time (days)	PLGA-GE Nanofibers	PLGA-GE-CH Nanofibers	PLGA-GE-CH-Que Nanofibers
1	0	41.78±2.76	43.42±1.8
3	0	20.4±3.53	25.63±2.57
5	0	12.52±4.05	16.71±3
7	0	8.4±2.950469	10.2±3.1

The values are expressed as mean±SD (n=3).

5.4.5. Free-radical scavenging efficiency of nanofibers

Antioxidant properties of the fabricated nanofibers were evaluated by DPPH scavenging efficiency of nanofibers and results are presented in Figure 5.36. The assay is based on the principle that DPPH is stable free-radical and it gives purple color solution in methanol. After accepting an electron or hydrogen from an antioxidant, it reduces to $DPPH_2$ and solution color changes to yellow. This change in color is measured at λ_{517nm} and utilized for estimation of relative antioxidant efficacies of different nanofibers [Selvaraj and Fathima 2017]. PLGA-GE nanofibers scavenged about 18.67% DPPH which was probably due to terminal –OH groups in PLGA and gelatin-derived radical-scavenging peptide sequence (His-Gly-Pro-Leu-Gly-Pro-Leu) [Mendis et al. 2005]. Further significantly higher scavenging efficiency (30.08%) of PLGA-GE-CH nanofibers attributed to higher release of ciprofloxacin hydrochloride from PLGA-GE matrix which also contains –OH groups. Similarly, significantly higher reduction of DPPH (61.89%) by quercetin and ciprofloxacin hydrochloride loaded nanofibers was due to additive effect of quercetin.

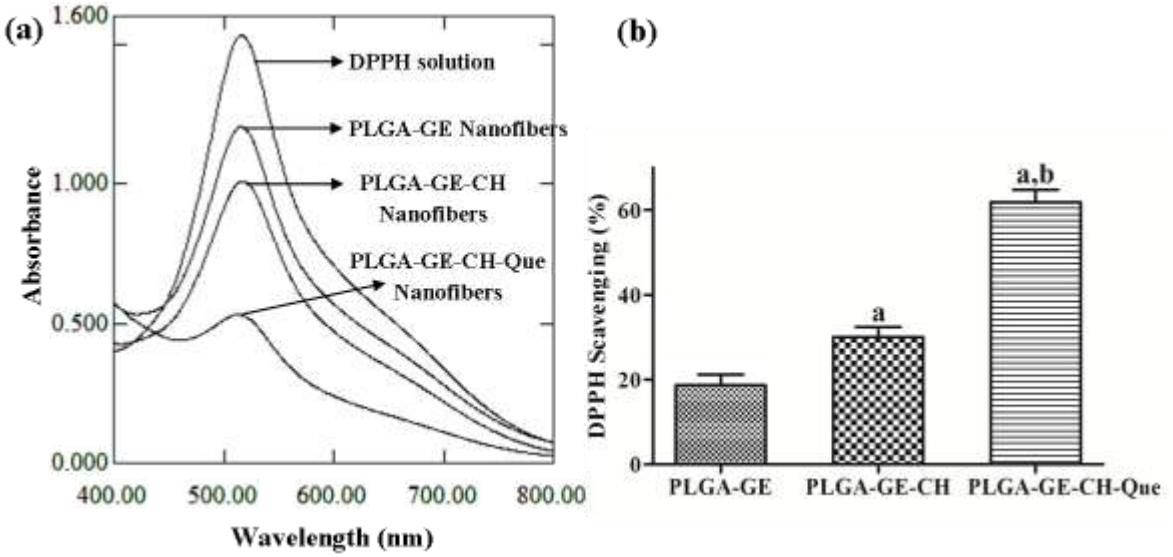

Figure 5.36: Free radical scavenging efficacies of the PLGA-GE, PLGA-GE-CH, and PLGA-GE-CH-Que nanofibers after 0.5h incubation with DPPH solution: (a) UV-Vis spectra; (b) histogram representing DPPH attenuation efficiencies of different nanofibers. $^{a}p < 0.05$ vs PLGA-GE nanofibers group, $^{b}p < 0.05$ vs PLGA-GE-CH nanofibers group. The data are expressed as mean and vertical bar represents SD (n=3).

5.4.6. Biocompatibility study

5.4.6.1. Hemocompatibility assessment of nanofiber membrane

Hemocompatibility of a scaffold anticipated for wound healing application is an essential requirement to preserve the integrity and functionality of RBCs in newly developed blood capillaries; otherwise it may cause some severe problem such as thrombosis. Percentage hemolysis denotes the magnitude of RBCs lysed when they are exposed to the nanofibrs. The hemolysis value of < 5% is considered as acceptable limit for the blood-compatible materials [Haghjooy Javanmard et al. 2016, Vatankhah et al. 2014]. As illustrated in Figure 5.37, the hemolysis caused by all three nanofiber membrane was under acceptable limit, which confirmed their blood-compatible nature. No significant difference were observed among their values, however low hemolysis caused by PLGA-GE-CH-Que nanofibers in comparisons to other nanofibers was attributed to protective action of quercetin, which

reduces the oxidative damage of unsaturated fatty acid, glutathione and thiol group (-SH) in RBCs membrane [Vijayakumar et al. 2016].

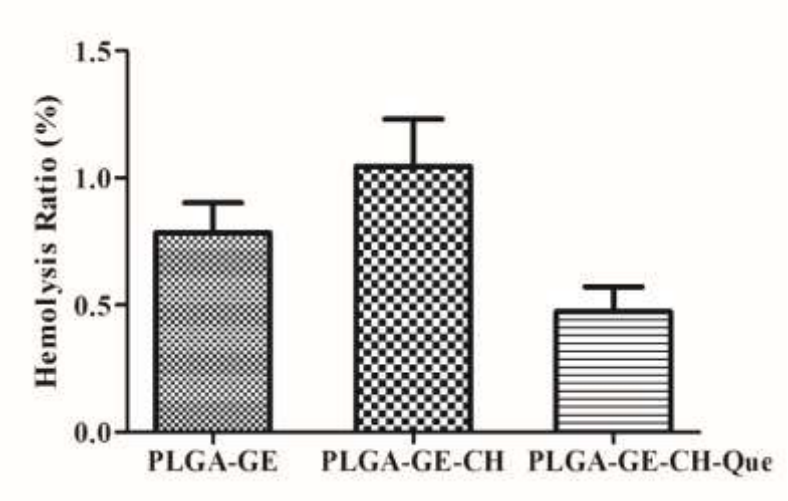

Figure 5.37: *In-vitro* hemocompatibility of PLGA-GE, PLGA-GE-CH and PLGA-GE-CH-Que nanofibers. The data are expressed as mean and vertical bar represents SD (n=3). No significant difference ($p>0.05$) was observed among their values.

5.4.6.2. Cytocompatibility assessment of nanofiber membrane

The viability of 3T6-Swiss albino fibroblast on fabricated nanofibers was examined by MTT assay and results are presented in Figure 5.38. It can be noted that most of the groups demonstrated more than 100% cell viability throughout the research period, which was attributed to Arg-Gly-Asp amino acid sequence available in gelatin protein. Arg-Gly-Asp amino acid sequence helped in fibroblast recognition, adhesion and proliferation on gelatin containing nanofibers. The possible reason for significantly ($p < 0.05$) higher cell viability on PLGA-GE-CH-Que nanofiber surface up to 48h was additional protective action offered by quercetin, a flavonoid. It has been reported that flavonoid increases the fibroblast proliferation and thus collagenesis [Selvaraj and Fathima 2017]. Therefore, the fabricated nanofibers allowed fibroblast proliferation on its surface which proves its cytocompatible and nontoxic nature.

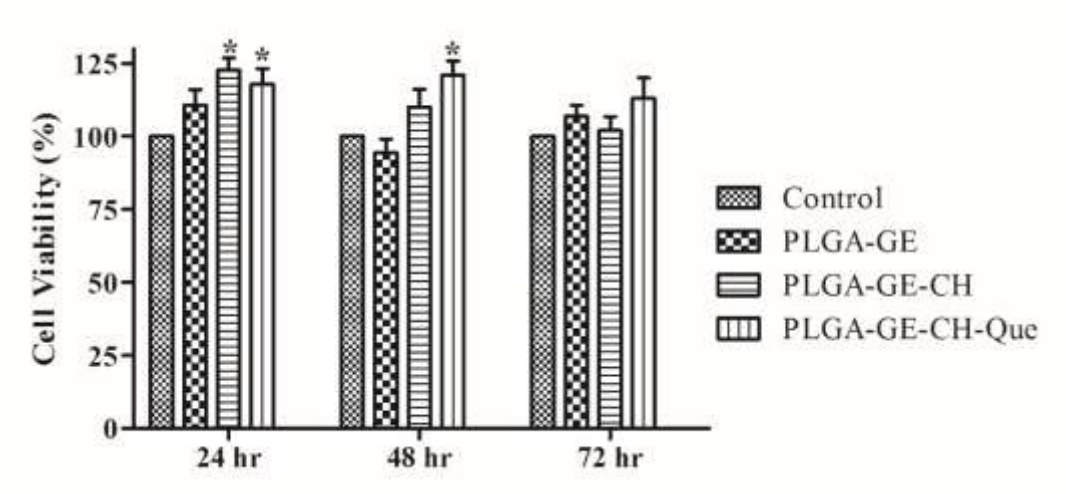

Figure 5.38: Viability of Swiss albino 3T6 fibroblast cells on nanofibrous scaffolds after 24h, 48h and 72h incubation times. The data are expressed as mean and vertical bar represents SD (n=3). *p < 0.05 vs control.

5.4.7. *In-vivo* wound healing study

Wound healing efficacies of fabricated nanofibers were examined by applying it on a circularly excised open wound, and the wound was left as such to heal by the secondary intention healing process. During the sixteen days of the healing period, post-operative adverse effects such as infection, sepsis, fluid retention, and bleeding of granulation tissues were not notice in the wounded area of treated animals. All the rats were alive throughout the study period, and displayed complete healing by the end of the third week. The representative images of all the four groups (gauze, PLGA-GE, PLGA-GE-CH, and PLGA-GE-CH-Que treated) animals with their healed wound area (%) with respect to time (days) are shown in Figure 5.39 (a) & (b), respectively. All the three nanofiber membrane were soft and flexible enough for wound application, and they conglutinate readily to the fresh wound surface. The 3D architecture provided by nanofibers and cell-recognition site (Arg-Gly-Asp amino acid sequence) on gelatin might have increased the cell recognition, and its proliferation on nanofibers surface, which resulted in significant healing in comparison to

gauze treated animals. On day 16, wound closed by PLGA-GE-CH-Que, PLGA-GE-CH, PLGA-GE and gauze treated group was 96.27%, 88.87%, 81.58% and 74.55%, respectively.

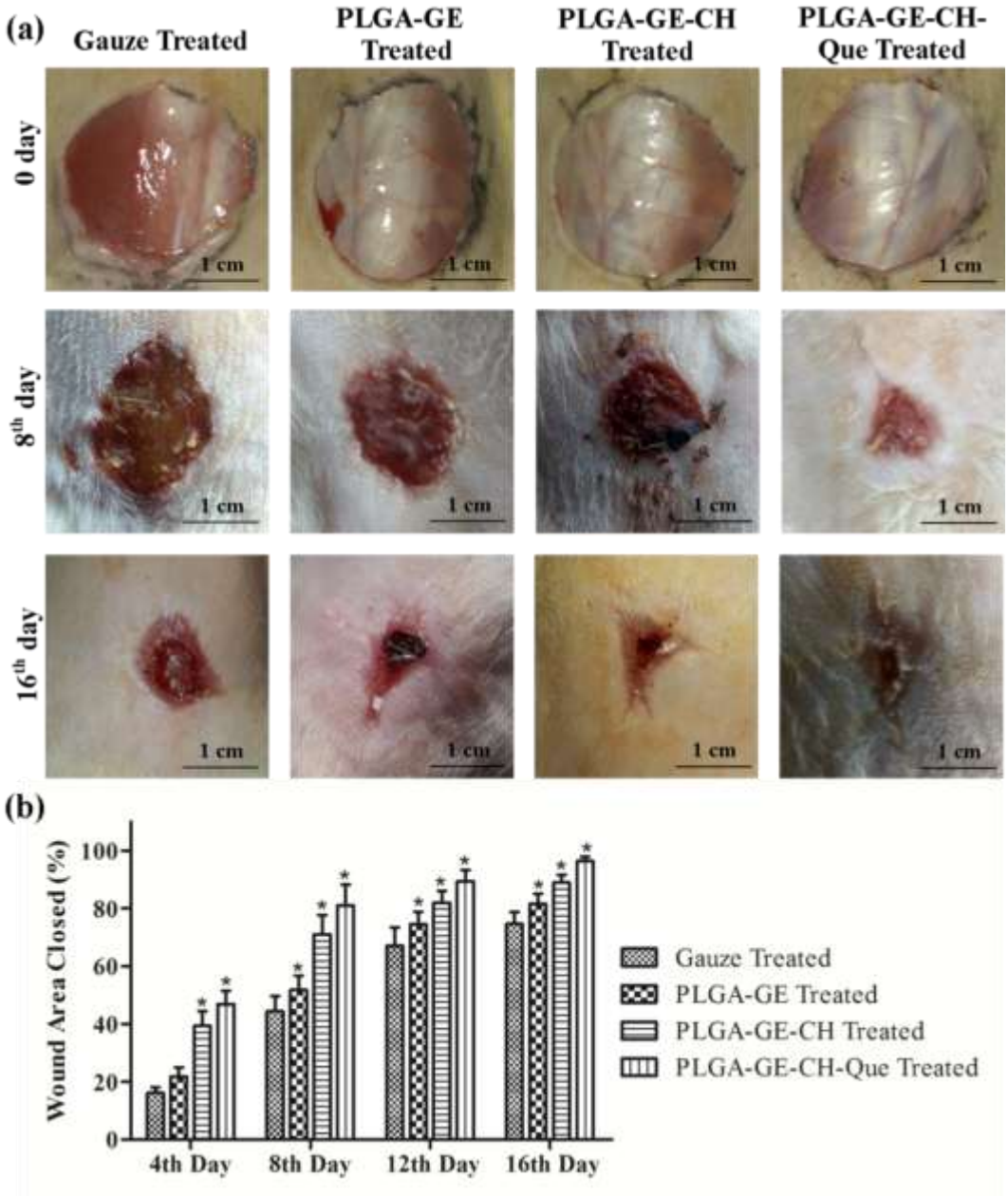

Figure 5.39: Healing Effect of nanofibers on full thickness wound: (a) representative images of wound healing on day 8 and 16, (b) percentage of wound area closed following treatment with gauze, PLGA-GE, PLGA-GE-CH and PLGA-GE-CH-Que nanofibers on day 4, 8, 12 and 16. The data are expressed as mean and vertical bar represents SD (n=3). *$p<0.05$ vs gauze treated.

5.4.7.1. Histological examination of granulation tissues

The histological changes in granulation tissues treated with gauze and different nanofibers was examined by hematoxylin & eosin staining and shown in Figure 5.40. On day 8, the underlying layer of granulated tissue treated with gauze and PLGA-GE nanofiber showed high infiltrated with inflammatory cells and highly ulcerated surface layer. In contrast, PLGA-GE-CH and PLGA-GE-CH-Que nanofibers treated group demonstrated moderate epithelialization, with relatively high collagen deposition in PLGA-GE-CH-Que nanofibers treated group. In the PLGA-GE-CH-Que treated group at this point the inflammatory response was relatively low compared to other group, which confirms its antioxidant activity.

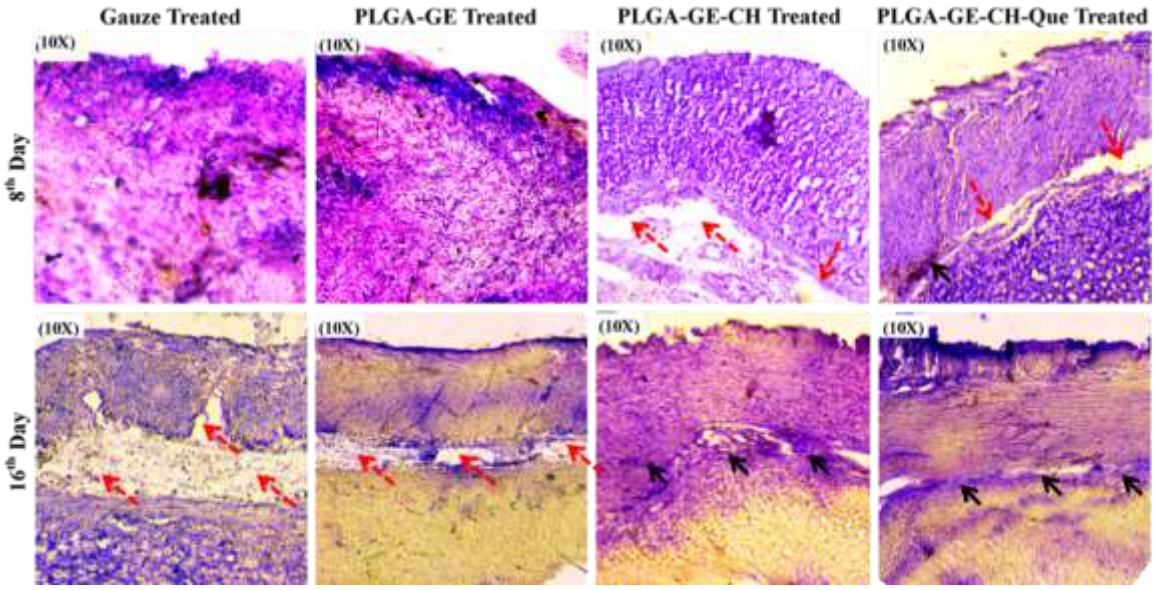

Figure 5.40: Histological changes in granulation tissue of gauze, PLGA-GE, PLGA-GE-CH and PLGA-GE-CH-Que nanofiber treated groups on day 8 and 16. Optical magnification was 10X. The black color arrow indicates growth of dermis and epidermis layer while red color arrow indicates lack of collagen synthesis in the dermis region.

On day 16, both PLGA-GE-CH and PLGA-GE-CH-Que nanofibers treated group achieved nearly complete re-epithelialization. Fewer white spot in PLGA-GE-CH nanofiber treated group indicated still lack of collagen deposition. Gauze and PLGA-GE treated groups showed moderate re-epithelialization with inflammatory infiltration, ulceration, necrotic fibrinoid debris, poor collagen deposition as indicated by larger by white space, and capillary hyperproliferation, signifying that inflammation still present in these groups.

5.4.7.2. Antioxidant enzyme activity in granulation tissues

Endogenous antioxidants (viz. SOD, catalase and glutathione) play important role in human physiology by balancing the free radicals (viz. ROS and RNS). However, in stress condition, such as open wound, excessive generation of free radicals causes oxidative damage of macromolecules. This condition requires supplementation of exogenous antioxidant to attenuate the exaggerated effect of ROS. Effect of exogenous antioxidant (viz. quercetin) on attenuation of free radicals and thus regaining of SOD and catalase level up to homeostatic state are shown in Figure 5.41. It was observed that after a week, PLGA-GE-CH-Que treated group achieved significant improvement ($p < 0.05$) in SOD and catalase level in comparison to other treated group, however, still a significant difference was found when compared with control group. This might be due to excessive inflammatory response during inflammatory phase which generally spans for 1-4 days. On day 16^{th}, only PLGA-GE-CH-Que treated group was able to regain the SOD and catalase level upto control group. At both time period, PLGA-GE-CH treated group was also capable to maintain a significant difference ($p < 0.05$) in comparison to gauze and PLGA-GE treated groups, however a significant difference was observed when compared with PLGA-GE-CH-Que treated group. Therefore, antimicrobial and antioxidant property of

nanofibers would be helpful for attenuating ROS and attaining the endogenous anti-oxidant level up to homeostatic state.

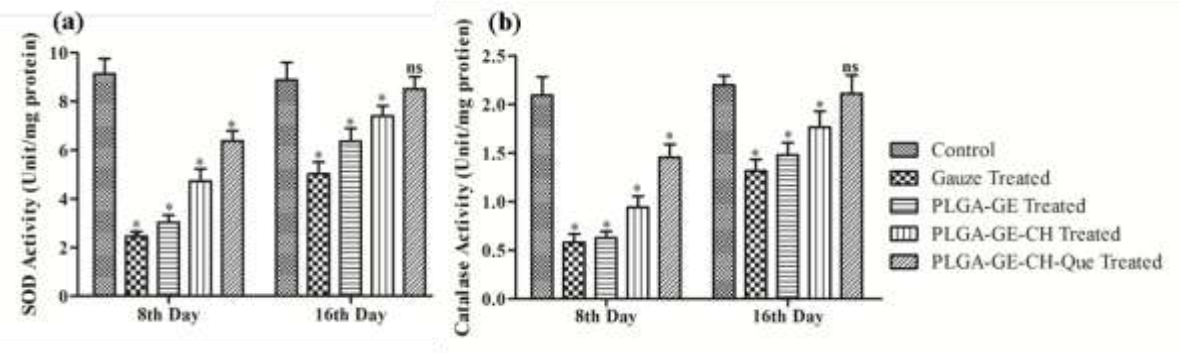

Figure 5.41: Effect of treatment with different nanofibers on endogenous enzymes viz. (a)SOD and (b) catalase in granulation tissues on day 8 and 16. The data are expressed as mean and vertical bar represents SD (n=3). *$p<0.05$ vs control group and $^{ns}p>0.05$ vs control group.

5.4.7.3. Hydroxyproline content in granulation tissues

The estimation of hydroxyproline in granulation tissues gives a direct indication of fibroblast activity or collagen deposition. The hydroxyproline content was determined as per method described by Reddy and Enwemeka, 1996, and results are shown in Figure 5.42. On 8^{th} day, although PLGA-GE-CH-Que nanofibers treated group achieved significant ($p<0.05$) improvement in hydroxyproline in comparison to gauze, PLGA-GE and PLGA-GE-CH treated groups; still a significant difference was observed when compared with control group. This significant improvement in PLGA-GE-CH-Que nanofibers treated could be attributed to pro-wound healing environment, such as prevention of microbial growth and hence low ROS generation, provided by nanofibers. On day 16, hydroxyproline content in PLGA-GE-CH-Que nanofibers treated group was found 2.505±0.189µg/mg of granulation tissue, and no significant difference was found when compared with the control group. Although, hydroxyproline content in PLGA-GE-CH

nanofibers treated group was quite close to PLGA-GE-CH-Que nanofibers treated (2.219±0.149µg/mg of granulation tissue), but still a significant difference exist between PLGA-GE-CH nanofibers treated group and control group. These findings show that quercetin addition had potentiated the healing property of nanofiber membrane by reducing fibroblast oxidation and, therefore, promoting collagen synthesis and speeding up the production of granular tissue.

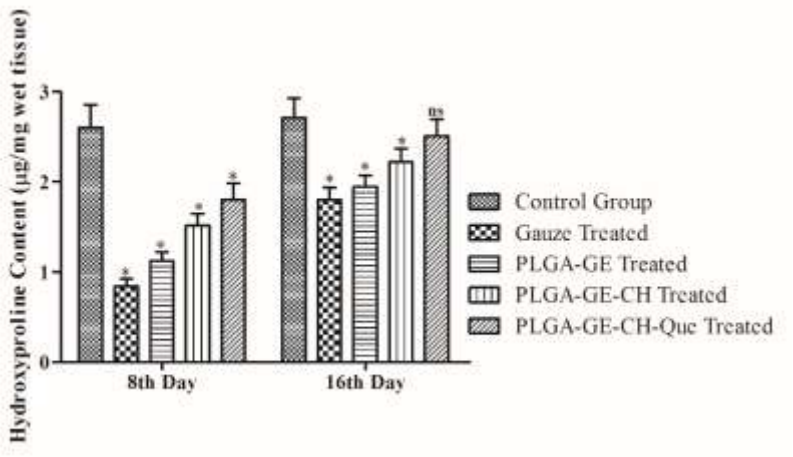

Figure 5.42 : Effect of different nanofibers on hydroxyproline content in granulation tissue of rats on day 8 and 16 post-wounding. The data are expressed as mean and vertical bar represents SD (n=3). *$p<0.05$ vs control group, and $^{ns}p>0.05$ vs control group.